Plasma Research Express

TUTORIAL

Electrical breakdown from macro to micro/nano scales: a tutorial and a review of the state of the art

Yangyang Fu[1,2], Peng Zhang[2], John P Verboncoeur[1,2] and Xinxin Wang[3]

[1] Department of Computational Mathematics, Science and Engineering, Michigan State University, East Lansing, Michigan 48824, United States of America
[2] Department of Electrical and Computer Engineering, Michigan State University, East Lansing, Michigan 48824, United States of America
[3] Department of Electrical Engineering, Tsinghua University, Beijing 10084, People's Republic of China

E-mail: fuyangya@msu.edu

RECEIVED
31 October 2019

REVISED
23 December 2019

ACCEPTED FOR PUBLICATION
16 January 2020

PUBLISHED
7 February 2020

Keywords: electrical breakdown, Paschen's law, secondary electron emission, thermionic emission, field emission, microdischarge, Townsend theory

Abstract

Fundamental processes for electric breakdown, i.e., electrode emission and bulk ionization, as well as the resultant Paschen's law, are reviewed under various conditions. The effect of the ramping rate of applied voltage on breakdown is first introduced for macroscopic gaps, followed by showing the significant impact of the electric field nonuniformity due to gap geometry. The classical Paschen's law assumes uniform electric field; a more general breakdown scaling law is illustrated for both DC and RF fields in geometrically similar gaps, based on the Townsend similarity theory. For a submillimeter gap, effects of electrode surface morphology with local field enhancement and electric shielding on the breakdown curve are discussed, including the most recent efforts. Breakdown characteristics and scaling laws in microgaps with both metallic and non-metallic (e.g., semiconductor) materials are detailed. For gap distance down to micro/nano scales, the breakdown characteristics and the breakdown mode transition from the secondary electron emission to the electric field emission or thermionic emission dominant regime. Additionally, the combined thermo-field emission regime is also reviewed. Previous efforts, including key simulations and experiments, have been devoted to diagnosing breakdown path evolution, measuring breakdown fields, and quantifying breakdown dependence on frequencies for gaps down to micro/nano scales. By summarizing and analyzing fundamental theories, recent progress, and on-going challenges, this tutorial review seeks to provide basic understanding and the state of the art of electric breakdown, which aids in advancing discoveries and promoting application prospects for discharge devices engineered in a wide range of regimes.

1. Introduction

Gas insulation has been widely used for a long time in systems where electrical breakdown is one of the most important issues due to many advantages, such as availability, recoverability, and effectiveness [1–3]. Electrical breakdown has thus been a continuously developed field in both academia and industry, with emerging challenges [4–7]. Electrical breakdown occurs if the applied voltage or electric field across a gap is sufficiently high to cause carrier multiplication through a number of mechanisms. The gas filled gap becomes electrically conductive when the gas neutrals are ionized to become charged particles. During gas breakdown, the gap voltage drops suddenly and the amplitude of the current flowing through the gap increases abruptly, which is the typical external electrical characteristic of the breakdown. There are many important factors, including gas pressure, gap distance, electrode geometry, gas type, and voltage waveforms, which have significant impact on the breakdown characteristics. It is generally recognized that electrical breakdown is more diffusive at low pressure while filamentary at high pressure, which can be explained with either Townsend or streamer theories, or their combinations in distinct regimes [8].

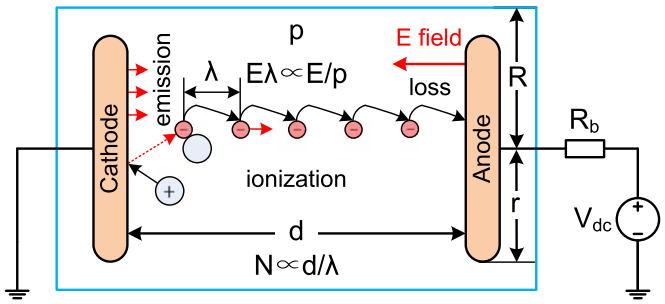

Figure 1. Illustration of the typical gas breakdown processes and key physical parameters. V_{dc} is an external voltage source and R_b is a ballast resistor.

The investigation of electrical breakdown in gases started shortly after the discovery of electricity. One famous publication can be dated back to 1889 when the German physicist F. Paschen conducted extensive experimental work on gas breakdown using a variety of gases and concluded that the breakdown voltage is a function of the combined parameter *pd* (gas pressure × gap distance), i.e., $V_b = f(pd)$, which resulted in Paschen's law [9]. In the early 1900s, the UK physicist Townsend established the Townsend theory, which addressed the fundamentals of gas discharge physics, including the Townsend breakdown avalanche process [10]. In 1915, in the book '*Electricity in gases*', Townsend illustrated that the ionization coefficient α is a function of the reduced electric field E/p, i.e., $\alpha/p = f(E/p)$, based on which Paschen's law can be explicitly derived [11]. The Townsend theory is mostly applicable at low pressure, especially for relatively small *pd* values. However, for very small *pd*, vacuum breakdown theory should be used. On the other hand, if the *pd* value becomes too large (i.e., $pd > 1200$ Torr·cm in nitrogen), fast breakdown processes occur with photoionization and streamer theory should be employed [8, 12, 13].

During the past one hundred years, gas breakdown in macroscale gaps has been studied with various focuses. The effects of gas mixture [14–17], electrode surface roughness [18–20], voltage waveforms [21–23], gas temperature [24–26], and electric field nonuniformity [27–30], on the breakdown characteristics have been extensively investigated by many researchers. Nowadays, emerging fabrication technologies enable electrodes with increasingly complicated geometries, and interelectrode distance down to micro/nano scales, allowing applications such as microplasma devices, microelectromechanical systems (MEMS), and nanoelectromechanical systems (NEMS) [31–37]. In this scenario, electron emission processes, such as thermionic or/and field emission, can have significant impacts on the breakdown characteristics, which would possibly provide new application opportunities. One of the most recent applications relevant to field emission driven breakdown is the ion-enhanced field emission triboelectric nanogenerator (TENG) designed for harvesting energy [38].

In this paper, fundamental theories of electrical breakdown are revisited with brief explanations. The dominant cathode processes, including secondary emission, field emission, thermionic emission, and their combined effects, are introduced for electrical breakdown under different conditions. Recent advances in scaling theory for electrical breakdown from macro to micro/nano scale gaps are surveyed with the consideration of better designing discharge devices. The key impact factors of electrical breakdown, such as electrode surface morphology, and breakdown characteristics, such as the modified Paschen's curve, are interpreted with detailed explanations. The breakdown scaling laws are also illustrated with cases from macro to micro scale. These results are beneficial for readers who wish to learn the state-of-the-art studies for electrical breakdown in gas gaps across a wide range of regimes.

2. Electrical breakdown fundamentals

2.1. Townsend theory

Electrical breakdown is a transient process in a gas filled gap when the gas changes from an insulator to a conductor, and is achieved by multiplication of primary electrons with electron avalanche and cascade ionization across the gap. Townsend established the theory of electrical breakdown in gases between two plane-parallel metal electrodes, as shown in figure 1. With an external voltage applied across the gap, the primary electrons near the cathode will be driven by the electric field, drifting from the cathode to anode and ionizing the background neutral gas atoms [39, 40]. As the number of electrons grows exponentially, positive ions are formed, which in turn move toward the cathode and produce secondary electron emission by impacting the

electrode surface. Townsend proposed three coefficients to describe these processes and combined them to derive the breakdown criteria.

The first Townsend coefficient α is the probability per unit length of path to ionize neutral gas atoms by electron impact collision , or equivalently, it is the number of collisions per unit length of path multiplied by the ionization probability per collision and is given as

$$\alpha = \frac{1}{\lambda_e} \cdot \exp\left(-E_i/\varepsilon_e\right), \tag{1}$$

where λ_e is the mean free path of electrons, E_i is the ionization threshold of the gas, and ε_e is the energy of the electron colliding with the gas atom [41, 42]. The mean free path of electrons λ_e can be estimated by $\lambda_e = k_B T/(\sigma_i p)$, where k_B is the Boltzmann constant, T is the gas temperature, σ_i is the electron impact ionization cross section, and p is the background gas pressure [42]. Assuming the electron energy gained from the electric field E between two consecutive collisions is $\varepsilon_e = eE\lambda_e$, the first Townsend coefficient α is expressed as

$$\alpha = A \cdot p \cdot \exp\left(-Bp/E\right), \tag{2}$$

where $A = \sigma_i/(k_B T)$ and $B = \sigma_i E_i/(ek_B T)$ are gas dependent constants, and e is the elementary charge [11, 43–45]. Note that here the electron mean free path λ_e is not distinguished from λ_E that is a projection of the electron free path along the electric field line. Equation (2) is typically applied when λ_E is smaller than the electron-neutral ionization path [46]. In case of uniform electric field, the electric field before breakdown is obtained as $E = V/d$, where V is the applied voltage on electrodes and d is the gap distance. Note that this field estimation is electrostatic and only applies in a pre-breakdown regime when the space charge effect is not important. If space charge effects are important, and the electron energy is in equilibrium with the local electric field, the spatial variation of the electric field distribution $E(x)$ should be considered, and the first Townsend ionization coefficient will also become spatially dependent, i.e., $\alpha(x)/p = f\left[E(x)/p\right]$. Note that the electron energy may not always synchronize with the electric field if the electric field gradient in space or time domain is sufficiently high, which is the so-called non-local effect, and more exact discussions can be found in [47, 48].

The second Townsend coefficient β describes the ionization caused by the positive ions during the breakdown, which was proposed in the early 1990s, which later was found to be less important since ion energy is relatively low and far below the threshold energy to effectively ionize the neutral gas [11, 43]. Therefore, generally $\beta \approx 0$ is assumed unless the ions have energies in hundreds to thousands of eV, which is not the case for low temperature gas discharge conditions. However, ions still have one critical role in sustaining the breakdown via impacting the cathode electrode and producing secondary electron emission. It is the so-called γ process, with $\gamma = \gamma_{se}$ being the third Townsend coefficient. The effective secondary emission coefficient γ_{se} is defined as electron emission due to all the impact particles bombarding a surface, including ions, metastable atoms, energetic electrons, and fast neutrals, i.e., $\gamma_{se} = N_{emit}/N_{incident}$ [49]. Note that even though the secondary electron emission can be caused by many different incident species, the ion impact secondary electron emission is generally the dominant one. The metastable induced secondary electron emission is less important since they are neutral and flowing by diffusion with relatively low energies. However, metastable induced secondary electron emission may be dominant when the electric field strength between pulses is weak. The electron induced secondary electron emission may occur under some specific circumstances, such as multipactor discharges, which is typically for vacuum or ultra-low-pressure breakdown conditions [50–52]. It can also be important for electron flux incident on drift tube walls, for example in a positive column in a glass discharge tube.

The ion induced secondary electron emission coefficient value will be larger if the ionization threshold of the gas is higher or the cathode work function is relatively lower. Generally, for a given gas and a cathode material, the coefficient γ_{se} depends on the energy of incident ions [53]. When the ions are bombarding the cathode surface, they are neutralized and give off their energy while some electrons are energized and released from the surface. For a given relatively large range of ion energy (i.e., $10^2 \sim 10^6$ eV), as shown in figure 2(a), the secondary electron emission coefficient first increases as the ion energy increases and reaches the maximum emission coefficient, which could be much larger than one, corresponding to the most effective energy. When the ion energy is further increased, the incident ions can penetrate deeper into the surface and only a small portion of the electrons are emitted, which results in a smaller secondary electron emission coefficient. However, the ion energy usually cannot be that high in gas discharge conditions. In figure 2(b), the secondary electron emission coefficient γ_{se} with all emission processes is shown as a function of the reduced electric field E/N, i.e., $\gamma_{se} = f(E/N)$, which was theoretically predicted and experimentally confirmed in Refs. [8, 54]. Here, $\gamma_{se} = \gamma_i + \gamma_m + \gamma_a + \gamma_{ph}$, where γ_i, γ_m, γ_a, and γ_{ph} are the emission coefficients correspond to the ions, metastable atoms, fast atoms, and photons [54, 55]. Three regions are mostly determined by the combination of the working gas and the electrode material. In the high E/N regime, the coefficient increases as the E/N increases, which is related to the ion energy gained from the electric field in one mean free path. In the low E/N regime, the emission coefficient increases as E/N decreases. This phenomenon would occur if the electron

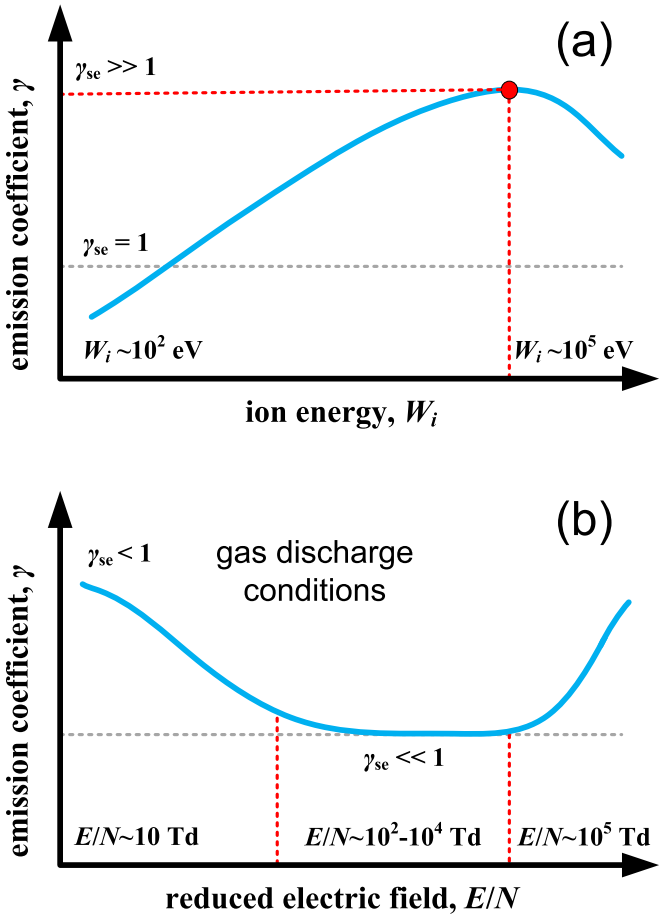

Figure 2. (a) Emission coefficient as a function of ion impact energy; (b) Effective secondary emission coefficient as a function of the reduced electric field; the coefficient is generally less than one in gas discharge conditions. More detailed information can be found in [54].

energy gain from the electric field is approximately the excitation E/N level of the gas, which induces more energetic species impacting on the cathode surface, resulting in a larger effective emission coefficient [8, 55, 56, 155]. The region between the low and high E/N regimes presents a minimum of emission coefficient. Often, the effective secondary emission coefficient is treated as a constant, independent of E/N, and the effective secondary electron emission coefficient is generally much less than one, i.e., $\gamma_{se} = 10^{-3} \sim 10^{-1}$ for gas discharge conditions. Note that here in figure 2(b), it just provides a general trend of the reduced electric field dependent effective secondary electron yield with all the emission processes (i.e., γ_i, γ_m, γ_a, and γ_{ph}) included, which might be very much different from the results from binary beam-surface collision experiments [54, 57]. Even though the effective secondary emission versus E/N is nonmonotonic, the ion-impact secondary emission generally increases as E/N increases [54]. In argon glow discharges, an apparent secondary electron emission coefficient versus E/N is given as $\gamma_{se} = 0.01(E/N)_c^{0.6}$, where $(E/N)_c$ is the reduced electric field at the cathode in the 3 kTd $\leqslant (E/N)_c \leqslant$ 20 kTd range (1 Td $= 10^{-21}$ V·m^{-2}) [58]. However, an empirical formula of the secondary electron emission due to the ion bombardment is also often used, i.e., $\gamma_{se} = 0.016(E_{iz} - 2\varphi)$, where E_{iz} is the ionization energy of the incident ions and φ is the work function of the electrode [59, 60]. Determining the secondary emission coefficient is far from being trivial, and it perhaps the least known data in a gas discharge since the incident angle, electrode structure, and surface status can significantly impact its value [61–63].

Combining the avalanche processes with the electron number growing exponentially and the secondary electron emission processes from the cathode, the total discharge current J represented by electrons at the anode is expressed as

$$J = \frac{J_0 \exp(\alpha d)}{1 - \gamma_{se}[\exp(\alpha d) - 1]}, \tag{3}$$

where J_0 is the initial current near the cathode surface, which could be contributed by cosmic rays [40, 43]. For a self-sustaining discharge, the discharge current J will still be non-zero even if the initial current J_0 vanishes, which requires the denominator to be zero, leading to the Townsend breakdown criterion as follows:

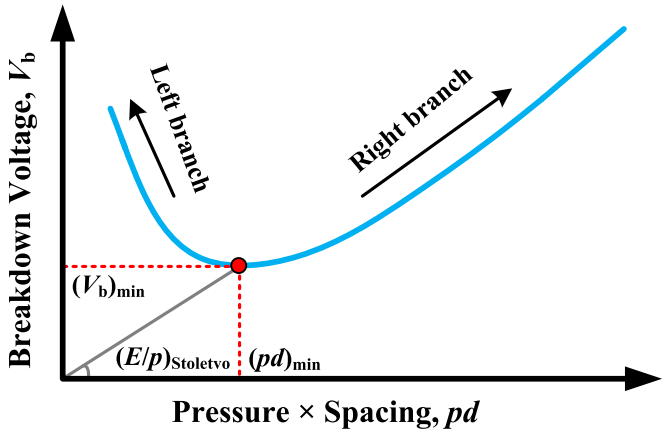

Figure 3. A general Paschen's curve for gas breakdown and an illustration of Stoletvo's constant.

$$\gamma_{se}[\exp(\alpha d)-1] = 1, \tag{4}$$

Since both γ_{se} and α depend on the reduced electric field formulated with an external applied voltage, the breakdown voltage can be obtained by solving equation (4). Note that if other loss mechanisms of the charged particles, such as attachment and diffusion loss, and the non-uniformity of the electric field are considered, an effective or a spatially dependent ionization coefficient α_{eff} can be employed in the breakdown criteria equation (4), i.e., $\alpha_{eff}(x) = \alpha(x)—\eta(x)$, where η is the coefficient for the loss term and x is the axial position. In this case, an integrated form is included in equations (3) and (4) and the breakdown criterion becomes

$$\int_0^d [\alpha(x) - \eta(x)]dx = \ln\left(1 + \frac{1}{\gamma_{se}}\right). \tag{5}$$

2.2. Paschen's law

In 1889 F. Paschen published a paper that introduced Paschen's law, which essentially states that the breakdown voltage V_b between two conductive materials is a function of the product of the gas pressure p and the gap length d, i.e., $V_b = f(pd)$ [9]. For simplicity, assuming a uniform electric field across the gap and substituting equation (2) into (4), the breakdown voltage V_b can be obtained from the Townsend breakdown condition

$$V_b = \frac{Bpd}{\ln(Apd) - \ln[\ln(1 + 1/\gamma_{se})]}, \tag{6}$$

where for a given working gas and cathode material, A, B, and γ_{se} are known [8]. The breakdown voltage as a function of pd is a 'V' shaped curve, called Paschen's curve, as shown in figure 3. Paschen's curve predicts very high breakdown voltage for small pd values, which corresponds to the left branch of the curve at low pressure or with short gap distance. As pd increases, a minimum breakdown voltage is reached. As pd is further increased, it enters the right branch of Paschen's curve, and the breakdown voltage also starts increasing as pd increases. On the left branch of the Paschen's curve, the breakdown voltage is usually more sensitive to the pd variation, showing a steeper slope. It should be mentioned that Paschen's curve can be measured by either changing the gap distance and gas pressure separately or dependently. Different parametric methods may result in different shapes of measured Paschen's curve even though the range of pd value is the same. Especially, if the measurement is carried out by changing the interelectrode distance d solely, without scaling the electrode radius r, the electric field could be altered significantly and no longer uniform when the aspect ratio d/r becomes large. In this case, the aspect ratio d/r acts as an additional parameter impacting the breakdown voltage and the breakdown scaling might not be strictly maintained, unless geometrically similar gaps are used.

According to equation (6), the minimum breakdown point is given by [41, 42]

$$(V_b)_{min} = \frac{\exp(1)B\ln(1/\gamma_{se})}{A}, \tag{7a}$$

$$(pd)_{min} = \frac{\exp(1)\ln(1/\gamma_{se})}{A}. \tag{7b}$$

From equations (7a) and (7b), we can have the ratio between the lowest breakdown voltage and the corresponding pd value

$$(E/p)_{\text{Stoletvo}} = \frac{(V_b)_{\min}}{(pd)_{\min}} = B \tag{8}$$

which is called the Stoletvo point [64]. Note that equation (8) is a convenient way to represent the Stoletov's constant B. More generally in discharge physics, the electron should be accelerated in the electric field to gain an energy $\Delta\varepsilon = e \cdot E/\alpha$ between two consecutive ionizations [8]. Combining $\Delta\varepsilon = e \cdot E/\alpha$ with equation (2), one can find that $\Delta\varepsilon$ is a function of the reduced electric field E/p. The minimum electron energy gained from the electric field is $\Delta\varepsilon_{\min} = \exp(1) \cdot eB/A$ at $E/p = B = (E/p)_{\text{Stoletvo}}$. As mentioned before, Stoletov's constant B is several times the gas neutral ionization threshold E_i, i.e., $B = A \cdot E_i$, indicating an optimal condition for gas ionizations in the reduced electric field.

The right and left branches of the Paschen's curve can be explained under extreme conditions. When pd is large, and the electron mean free path $\lambda \sim 1/p$ and/or the electric field $E \sim 1/d$ for a given applied voltage V are very small, then the mean electron energy $\tilde{\varepsilon} = eE\lambda \sim V/(pd)$ gained from the electric field between two consecutive collisions might be much less than the gas ionization energy threshold. This condition requires a higher applied voltage with a stronger electric field to ignite the breakdown. On the other hand, if pd is too small, when electrons travel from the cathode to the anode, the average number of electron-neutral collisions, $N_{\text{collision}} = d/\lambda \sim pd$, would also be very small, which indicates a lower chance of ionizing the gas. In this case, relatively high breakdown voltages are also required. A higher breakdown voltage is needed for either a very high or very low pd value, which results in the minimum breakdown voltage between the right and left branches of the Paschen's curve.

The pd regime and the lowest point of Paschen's curve is critical for many practical applications [65, 66]. Taking the fluorescent light bulb or spark plug as examples, their working conditions can be designed to match Paschen's curve minima , operating with lower power consumption. Besides that, the pd scaling law can also predict the length scales of the discharge at different pressure regimes. The scaling predicts that to avoid arc discharges, low-temperature microplasmas should operate around micrometer scales at atmospheric pressures [67–69].

It should be further noted that at very low or very high pressures, Paschen's law might not be valid. At very low pressures, Paschen's law predicts infinite breakdown voltage, which is not the case since the field emission can occur to initiate a breakdown under sufficiently high electric field independent of the gas pressure. At very high pressures, streamer mechanisms should be employed in the region where the breakdown is not determined only by pd. For a highly non-uniform electric field, corona discharge with a localized breakdown should be considered. Besides that, the effects of the gas temperature and gas flow on Paschen's curve are also very important under specific conditions [24]. In this paper, breakdown is discussed with gas temperature below the threshold for thermal ionization and the effects of the other possible mechanisms, such as flow turbulence, photoionization and laser induced ionizations, are not within the scope.

2.3. Electrode surface emissions

As discussed before, the discharge can be self-sustained with ion impact secondary electron emissions from the cathode. However, under certain conditions, other surface emission processes may occur, resulting in significant impacts on the Paschen's curve. These processes include thermionic emission, electric field emission, and combined thermo-field emission.

When a metal is heated, electrons can acquire enough energy to overcome the potential well. The thermionic emission current density J_{T} is given by the Richardson–Dushman expression

$$J_{\text{T}} = A_R T_s^2 \exp\left(-\frac{\text{e}\Phi_{\text{w}}}{k_B T_s}\right), \tag{9}$$

where A_R is the material-dependent constant, T_s is the electrode surface temperature, Φ_{w} is the electrode work function [8]. With an additional external electric field E_0, the emission will be enhanced with the effective work function reduced to $(\Phi_{\text{w}})_{\text{eff}} = \Phi_{\text{w}} - \sqrt{e^3 E_0/\varepsilon_0}$, which is the Schottky effect [70].

When an external electric field is applied to a non-heated metal, the electron potential energy profile near the metal surface becomes triangular and if the electric field is sufficiently high, the electrons can escape from the metal by tunneling [71]. It is called the field emission process and the emission current density can be given by the Fowler-Nordheim (FN) formula

$$J_{\text{FN}} = \frac{A_{\text{FN}} E_S^2}{\Phi_{\text{w}}} \exp\left[-\frac{B_{\text{FN}} \Phi_{\text{w}}^{3/2} \upsilon(y)}{E_S}\right], \tag{10}$$

where A_{FN} and B_{FN} are material dependent constants, E_s is the electric field of the cathode surface, $\upsilon(y)$ is with dependence on the external electric field and work function [49, 71]. With the electric field applied on the heated cathode, both thermionic and field emission would occur and generate thermionic field emission current, which may not be expressed by simple formulas. In the 1950s, the Murphy-Good expression was developed with

complex integrations to describe over the thermo-field regime [72]. In the past decade, Jensen *et al* derived a more tractable analytical model, i.e., thermal-field-photoemission equation, incorporating the thermionic emission, field emission, and photoemission in distinct domains [73–75]. Generally, we may expect that at high temperature and low electric field, the thermionic emission is dominant while at low temperature and strong electric field, field emission is important. The thermo-field emission should be employed for the transition regimes in which the contributions from the two sides are comparable [72–75, 156].

Thermionic and electric field emission have a critical impact on the breakdown characteristics. With the thermionic and electric field emission considered, the total current with the electron impact ionization during the breakdown process is expressed as

$$J = \frac{J_{\text{emit}} \exp(\alpha d)}{1 - \gamma_{\text{eff}} [\exp(\alpha d) - 1]}, \tag{11}$$

where the emitted current is $J_{\text{emit}} = J_0 + J_{\text{T}} + J_{\text{FN}}$ and the effective secondary electron emission is defined as $\gamma_{\text{eff}} = J_{\text{emit}} / J_{\text{incident}}$ [49]. Compared to the ion induced secondary electron emission case, this effective secondary electron emission is significantly enlarged due to thermionic and field emission, which will greatly decrease the breakdown voltage, deviating from the prediction of the classical Paschen's law [76–78].

3. Macroscale electrical breakdown

3.1. Breakdown quantification

The electrical breakdown may not instantly occur when an external voltage is applied across two electrodes in gases. This could be caused by either a breakdown time delay or an applied electric field below the breakdown threshold. The breakdown process can develop either abruptly or progressively. Zuber and von Laue proposed a statistical description for gas breakdown using probability distribution functions [79, 80]. From a statistical prospective, the electrical breakdown voltage is considered as the maximum voltage at which an electrical system can operate without any breakdown events, or equivalently, at which the breakdown probability is zero. In [81], an expression of the breakdown probability W is given as

$$W = 1 - \frac{1}{\gamma_{\text{se}} [\exp(\alpha d) - 1]}, \tag{12}$$

which is consistent with the Townsend breakdown criteria when W is zero. Equation (12) is defined as $W = 0$ for $\gamma_{\text{se}} [\exp(\alpha d) - 1] < 1$ [81].

From the experimental perspective, the most accurate breakdown voltage is the smallest voltage at which breakdown has ever been detected. The two determinations are naturally consistent. To obtain the onset voltage corresponding to breakdown in experiments, the applied voltage is usually increased at a certain rate from a small to a sufficiently high electric field to initiate the electron avalanche and achieve a complete breakdown. It was previously confirmed that the breakdown voltage is a function of the voltage increase rate, as is shown in figure 4 [81]. The breakdown voltage is found to be increasing as the rate k increases. The rate of increase of the applied voltage should be small enough to avoid the overshooting onset of breakdown. The static breakdown onset can be estimated by extrapolating the experimental data to zero. In figure 4(a), the voltage rise rate k varies from 10 to 100 $\text{V}\cdot\text{s}^{-1}$ and estimated static breakdown is about 415 V. However, in figure 4(b), it is predicted as 390 V with k ranging from 1 to 12 $\text{V}\cdot\text{s}^{-1}$. It was concluded that the prediction of the static breakdown voltage is more precise if the rate of increase of the applied voltage is lower [81, 82]. However, for a long discharge tube, the dependence of the breakdown voltage on the voltage rise rate could be more complicated due to the surface charge accumulation on the tube wall. In Ref. [83], a nonmonotonic dependence of the breakdown voltage on the voltage rise rate was experimentally observed in an 80-cm long discharge tube at low pressure, which showed that the breakdown voltage could be higher when the voltage rise rate is smaller. This phenomenon was attributed to increased surface charge accumulation with a small voltage rise rate which reduced the potential difference between the electrode and the wall, requiring a higher applied voltage [83–85].

More recently, Levko *et al* analyzed the influence of the voltage rise time on Paschen's curves under pulsed breakdown conditions [86]. They found that with decreasing voltage rise time, the minima of Paschen's curves shifts toward the right-top corner, which is further qualitatively confirmed by the computational results based on kinetic, fluid and analytical models [86]. The phenomena of modified Paschen's curves are attributed to the ion impact secondary electron emission and electron multiplication having insufficient time to develop when the applied voltage is rising too fast.

Another method for quantifying the breakdown voltage is based on the voltage-current characteristics of a discharge, which usually shows a transition from Townsend to subnormal and normal glow discharge regimes [87–89]. This transition characteristic of the voltage-current curve was found in discharges from low and high pd regimes by experiments, which can be used to quantify the Townsend breakdown voltage and obtain Paschen's

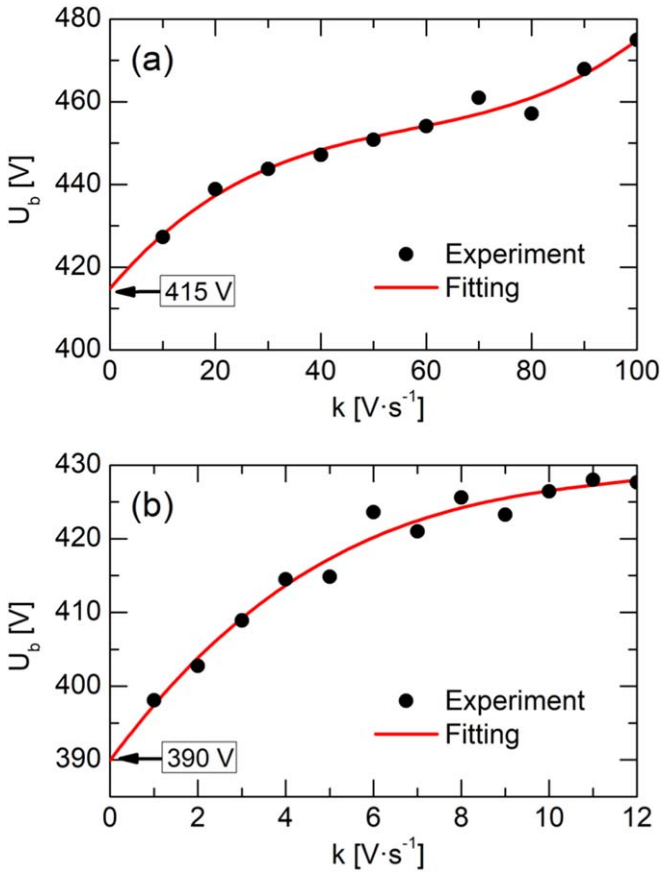

Figure 4. Breakdown voltage as a function of the rate k of increase of the applied voltage in a nitrogen-filled tube at 4.0 mbar. (a) The voltage rise rate k varies from 10 to 100 V·s^{-1}; (b) The voltage rise rate k varies from 1 to 12 V·s^{-1}. Reproduced with the permission of IOP Publishing from [81].

curve with both left and right branches [87, 90]. This method was also employed to quantify the breakdown voltage for macro and submillimeter gaps when the ion impact secondary electron emission is dominant [91]. In the field emission regime, a smooth transition from a pre-breakdown to a self-sustained condition is observed, based on which the breakdown voltage can also be estimated [88]. In the field or thermionic emission regimes, discharge current usually increases exponentially as the gap voltage increases, and the breakdown can also be recognized by the slope of the voltage-current plot [92, 93]. Note that the breakdown voltage may differ due to the fluctuations of the discharge conditions, which could be caused by aging effects, memory effects, and incident pulse shapes [94–97].

3.2. Breakdown similarity laws

Paschen's law indicates that under a uniform electric field, for various discharge gaps with different values of gas pressure and gap distance, the breakdown voltage will be the same if the product pd is kept the same. According to Townsend's book '*Electricity in Gases*', Paschen's law is only one special case of the similarity principles in a gas discharge, specifically for uniform electric field conditions [11]. However, the breakdown scaling could be extended to nonuniform conditions according to similarity laws based on the Townsend theory. The extended similarity laws are usually adopted for the breakdown in geometrically similar gaps, where the linear dimensions (d_x, d_y, and d_z) in every direction are in proportion, i.e., $d_{1j} = d_{2j}/k_s, j \in [x, y, z]$ with k_s being a scaling factor. Between parallel circular plates, the geometrically similar gaps are defined as $d_1/d_2 = r_1/r_2 = \ldots = k_s$, where the parameters ($d_1$, d_2, …) and (r_1, r_2, …) are interelectrode gap distance and electrode radius in the compared gaps. Besides, in the similar gaps the product of the linear dimensions and the gas pressure is kept the same, i.e., $p_1 d_1 = p_2 d_2$ and $p_1 r_1 = p_2 r_2$, which maintains the reduced electric field the same with the same gap voltage applied. The Townsend similarity law for gas breakdown is illustrated by $V_b = f(pd)|_{\text{geometrically-similar-gaps}}$, without requiring the electric field being uniform, which was verified in our previous works and many others for a wide range of geometric systems [98–105].

For plane-parallel interelectrode gaps, Paschen's curve is found to be sensitive to the gap geometry, as shown in figure 5 for parallel circular electrodes [98]. Parameters d, r, and R are the gap distance, the electrode radius,

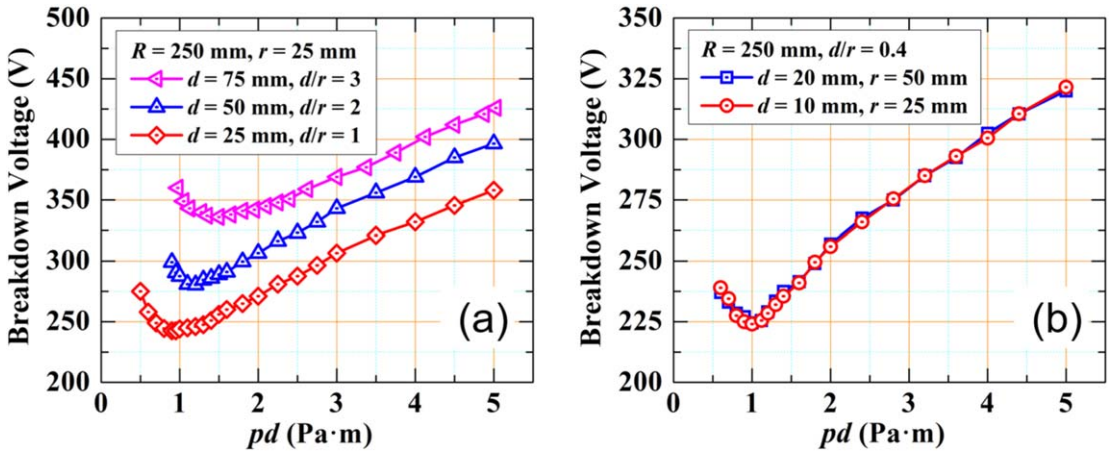

Figure 5. Breakdown voltage versus *pd* for parallel circular electrodes. (a) Paschen's curves moving upwards and rightwards with the increase of d/r; (b) Paschen's curves overlap with $d/r =$ const. Data extracted from Ref. [98].

and the radius of the discharge chamber housing the electrodes, respectively. The breakdown was measured under DC voltage and the breakdown voltage was determined by the abrupt drop of the gap voltage. A slow growth rate of the applied voltage of about 1 V/s was used and the breakdown voltage was measured with an accuracy of $\pm$ 2 V. In figure 5(a), Paschen's curves are separated and move upwards and to the right with an increase of d/r, which indicates the breakdown voltage should be described by $V_b = f(p, d)$ rather than $V_b = f(pd)$. It means Paschen's law may not be valid for the case when the electrode radius does not scale proportionately with the gap distance. In figure 5(b), the electrode radius and the gap distance scale accordingly with an equal value of d/r, resulting in overlapping Paschen's curves. It is concluded that the breakdown voltage should be given by $V_b = f(pd, d/r)$, which is equivalent to $V_b = f(pd)|_{d/r=\text{constant}}$. Here $d/r =$ constant is an expression for defining the geometrically similar gaps with all the dimensions scaled simultaneously, which further confirms that the expressions $V_b = f(pd)|_{\text{geometrically-similar-gaps}}$ and $V_b = f(pd)|_{d/r=\text{constant}}$ are fundamentally equivalent. For plane-parallel gaps, the static electric field distributions in the axial direction are primarily determined by the aspect ratio d/r. It is considered that the $d/r =$ constant $\neq 0$ corresponds to nonuniform electric field cases, while $d/r =$ constant $\rightarrow 0$ corresponds to uniform electric field cases. Therefore, it is confirmed that no matter whether the electric field is uniform or not, the breakdown voltage versus *pd* will follow the Townsend similarity laws if the gaps are geometrically similar, i.e., $V_b = f(pd)$. The physical meaning of the Townsend breakdown similarity laws is clear. For geometrically similar gaps, the breakdown voltages are the same if $p_1 d_1 = p_2 d_2$, indicating the mean number of collisions of an electron traveling from the cathode to the anode during an avalanche are the same. With the same applied voltage, the reduced electric fields at the corresponding position ($p_1 x_1 = p_2 x_2$) in two geometrically similar gaps can be further proved to be the same, i.e., $E_1(x_1)/p_1 = E_2(x_2)/p_2$, which indicates the mean energy gained by an electron between two corresponding collisions is the same [106, 107]. More generally, under the same applied voltage, the ionization processes and the charge fluxes towards the electrodes in geometrically similar gaps are proportional, resulting in the same total discharge current, the same voltage current characteristics, and the same distribution of surface charges, which is the original definition of similar discharges by Holm [108].

As for alternating current (AC) conditions, Lisovskiy *et al* measured and analyzed the RF breakdown voltages with respect to the gap distance and voltage frequency in Ref. [109]. The RF breakdown curves in nitrogen with various gap distance are not entirely overlapping and only coincide towards the right branch, as shown in figure 6(a), where U_{rf} is the RF breakdown voltage, f is the frequency, p is the gas pressure, L is the gap distance, L/R is the aspect ratio of the gap. In figures 6(b) and (c), the combined parameter fL is kept the same for the compared gaps, where the gap distances are 23 mm and 11.5 mm and frequencies are 13.56 MHz and 27.12 MHz, respectively. Paschen's curves overlap in the whole fL range. It was concluded that the breakdown voltage should be described as $U_{rf} = f(pL, L/R, fL)$. They claimed that the impact of L/R becomes important and acts as an additional factor for the breakdown in non-geometrically similar gap when $L/R > 0.4 \sim 0.5$ [105]. The extended breakdown voltage expression $U_{rf} = f(pL, L/R, fL)$ still follows the prediction of Townsend similarity theory, which includes fL, fR, and f/p as similarity parameters for alternating current discharges, as introduced in the book by Francis [44].

Note that the parameter f/p is not suitable for description of multipactor discharges, which is independent of gas pressure, and the invariant fL was suggested, which ensures the electron kinetic energy is the same for similar discharges [109, 110]; for gas discharges, f/p and fL are equivalent with pL being invariant in compared systems

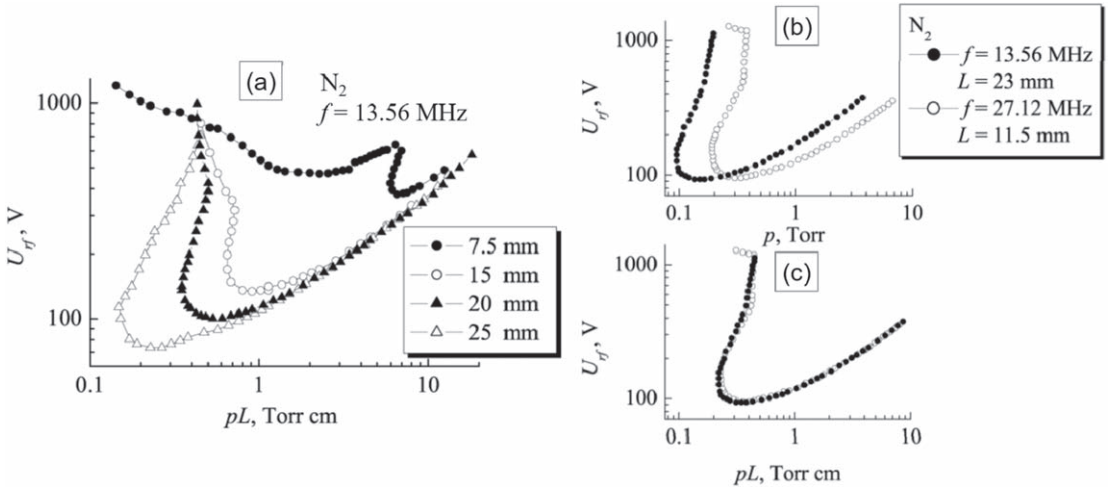

Figure 6. The experimentally measured RF breakdown curves in N_2. (a) RF breakdown voltage U_{rf} versus pL with $f = 13.56$ MHz; (b)-(c) RF breakdown voltages with $f = 13.56$ MHz, $L = 23$ mm and $f = 27.12$ MHz, $L = 11.5$ mm and plotted as a function of p and pL, respectively. Reproduced with the permission of IOP Publishing from [109].

[109, 111]. Comparing to the clear physical meaning of E/p in gas discharges, f/p or fL is not that straightforward . According to the previous work, two quantities having the dimension of energy, i.e., $\varepsilon_1 = eE\lambda$ and $\varepsilon_2 = m(f\lambda)^2/2$, should be invariant in similar discharges [106]. The former expression is readily satisfied if the reduced electric field is the same; the latter one reflects the necessity of the frequency scaling, i.e., $f\lambda \sim f/p$, which indicates a velocity dimension independent of systems. In gas discharge systems, it can be generally considered that the invariant fL maintains the same number of collisions within a certain time period while the invariant pd ensures the same number of collisions per certain distance [112]. More specifically, in RF discharges the reduced effective electric field E_{eff}/p is usually used and expressed as

$$\frac{E_{\text{eff}}}{p} = \frac{E_{\text{rms}}}{p} \cdot \frac{\nu_{\text{en}}}{\sqrt{\nu_{\text{en}}^2 + \omega^2}} = \frac{E_{\text{rms}}}{p} \cdot \frac{\nu_{\text{en}}/p}{\sqrt{(\nu_{\text{en}}/p)^2 + (2\pi f/p)^2}}, \tag{13}$$

where $E_{\text{rms}} = E_{\text{rf}}/\sqrt{2}$ is the root mean square value of applied RF field E_{rf}, ν_{en} is the electron-neutral collision frequency, and $\omega = 2\pi f$ is the angular frequency of the RF voltage [109]. Equation (13) also indicates that if the reduced electric field remains the same, the collision frequency should be scaled with gas pressure, which was widely confirmed in previous studies [44, 106, 109–112]. During the early stage of the breakdown process, electron-neutral collisions are the dominant ionization mechanism, which is considered as a linear process in terms of the scaling law. However, as the breakdown develops, the nonlinear ionization processes (e.g., three-body collisions) could possibly have a negative impact on the validity of scaling laws, especially for steady-state discharges at high pressure [113–115].

The breakdown scaling was also studied with the non-geometrically similar gaps and Paschen's law may not be strictly valid since the electric field may not be uniform [116]. Figure 7 shows the measured Paschen's curves with different aspect ratios, which do not superimpose . The gap distance is fixed at 60mm and the relative position of the breakdown voltage curve as a function of p and pd is the same. The electrode radii are 30 mm, 15 mm, 5 mm, 3 mm, which correspond to aspect ratios d/r of 2, 4, 12, and 20, respectively. As d/r increases, the non-uniformity of the electric field is generally aggravated. By considering different distributions of electric field, the intersection behavior of Paschen's curve in figure 7 was reproduced with the different gap aspect ratios [116]. This result, in turn, confirms the necessity of the requirement of geometrically similar gaps for the application of Townsend similarity laws when the electric field is not uniform.

4. Microscale electrical breakdown

4.1. Submillimeter scale breakdown

During recent decades, there has been growing attention to microdischarges or microplasmas, which have a characteristic length less than one millimeter. According to the pd scaling law, shrinking the electrode distance to submillimeter regimes is a typical method to generate low-temperature plasma discharges, avoiding long-distance arc discharges, especially at atmospheric pressure [67, 68]. The breakdown processes for microplasma formation are of great interest due to their impact on system variability, energy efficiency, stability, and many other aspects. It is generally considered that in the submillimeter regime, low-temperature plasma formation is still dominated by

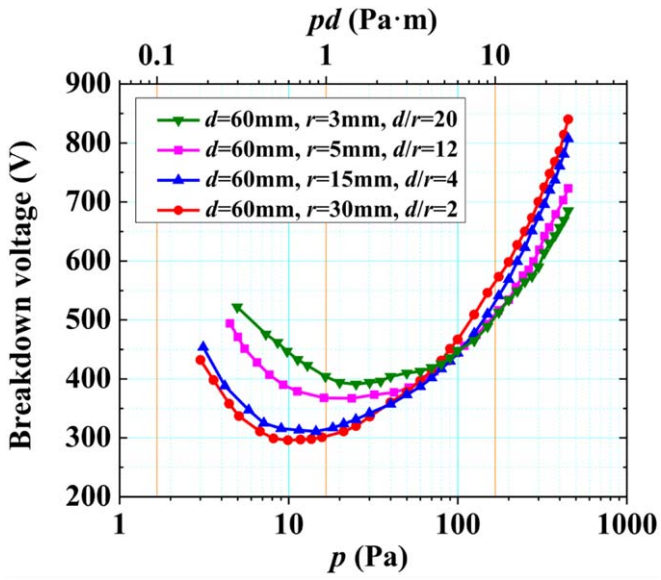

Figure 7. The intersection of Paschen's curves in argon. Reprinted with the permission of AIP Publishing from [116]. Copyright 2016 AIP Publishing LLC.

secondary electron emission, which can still be interpreted by Townsend theory [91]. With the *pd* value being high enough, the breakdown is a streamer process beyond the Townsend regime. Recent advances enable manufacturing of devices with increasingly complicated surface morphologies on the electrodes to further control plasma characteristics. One significant concern is the effect of surface roughness on the microgap breakdown since having an ideal surface finish of electrodes in micro-systems is rather difficult. Besides that, the surfaces roughness may also be introduced from 'scratch-and-dig' during handling and assembly procedures. Therefore, exploring the effects of electrode surface morphology on the microscale breakdown processes is of critical importance for optimizing the device voltage hold-off and electrical variability.

The effects of designed surface morphologies on electric breakdown in submillimeter regimes have been numerically investigated in Refs. [117–120]. It is found that in microgaps, Paschen's curve can be flattened with electrode surface protrusions, and in millimeter and centimeter gaps, similar phenomena are observed in the experiments [121, 122].Breakdown voltages in microgaps were measured based on the voltage-current characteristics, showing a transition from the Townsend to subnormal glow regime. When single or multiple micro-protrusions were introduced on the cathode electrode in microgaps, breakdown can be significantly affected by the breakdown path, electric field distortions (local field enhancement and divergence of field lines) and effective cathode emission areas [119, 120]. In figure 8, Paschen's curve obtained with a single surface protrusion on the cathode (case 3) was compared to the other two curves for plane-parallel electrodes (case 1 and 2), as shown. Cases 1 and 2 are gaps with plane–parallel electrodes and gap distance at 50 μm and 500 μm, respectively, and define the minimum and the maximum gap distance in case 3 with the presence of a surface protrusion (450 μm in height and 200 μm in radius) on the cathode. The minima of Paschen's curve for case 1 is located at higher-pressure compared to case 2. While in case 3, with a surface protrusion introduced on the cathode, it results in a combined Paschen's curve that is generally determined by the left branch of case 1 and the right branch of case 2, transiting from a long-gap behavior at low pressure to a short gap behavior at high pressure, and keeping the breakdown voltage roughly constant and relatively low across a wide range of gas pressure. This combined Paschen's curve is due to the migration of the major discharge path between the electrode and protrusion when the gas pressure changes. The breakdown occurs between the anode and the protrusion tip (path I) at high pressure. The breakdown path automatically moves to the protrusion's side surface (path II) when the pressure decreases, and ends at the wider non-protrusion electrode substrate (path III), as shown in figure 8(a). The phenomena can be explained by the mean free path, λ, of electron–neutral collisions which is inversely proportional to the gas pressure. As the pressure decreases, the breakdown tends to automatically optimize to a longer path proportional to the gas pressure to acquire more collisions, maintaining the breakdown almost a constant in the flattened regime, as shown in figure 8(b).

The effect of multiple surface protrusions on the cathode is further discussed in Ref. [120]. In this scenario, the electric shielding effect might be important if the neighboring protrusions are located close to each other. With a strong shielding effect, the breakdown cannot reach the cathode substrate, i.e., a longer breakdown path is prohibited while a shorter breakdown path is reinforced, which results in a Paschen's curve close to

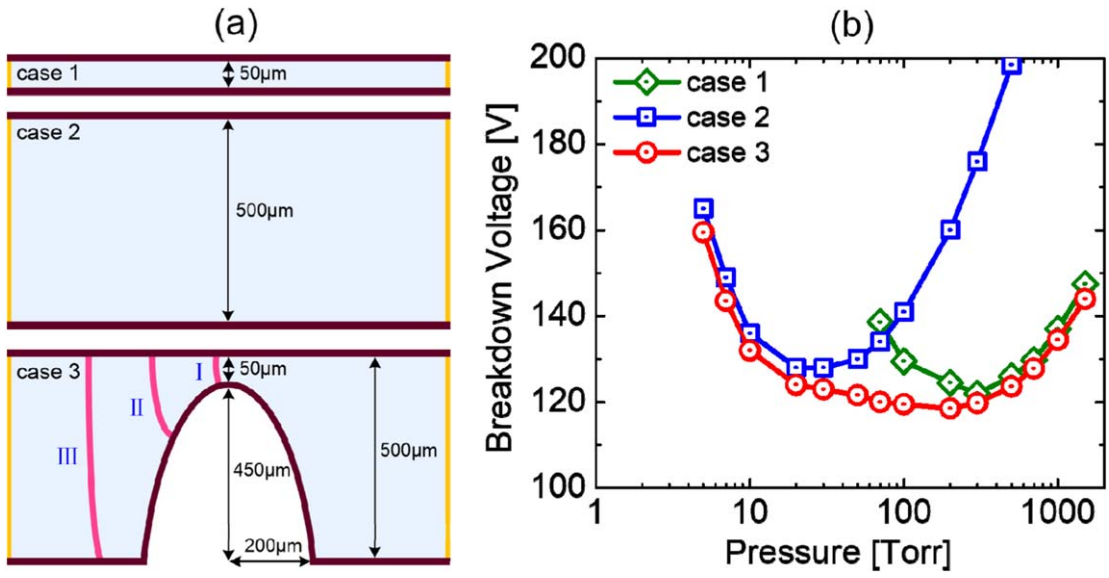

Figure 8. (a) Cases 1 and 2: plane–parallel electrode with a gap distance at 50 μm (short gap) and 500 μm (long gap), respectively; case 3: plane–parallel microgap with a hemiellipsoidal protrusion (450 μm in height and 200 μm in radius) on the cathode. (b) Calculated Paschen's curves for case 1, 2, and 3 with $R = 1000$ μm. Reprinted with the permission of IEEE Publishing from [119]. Copyright 2019 IEEE.

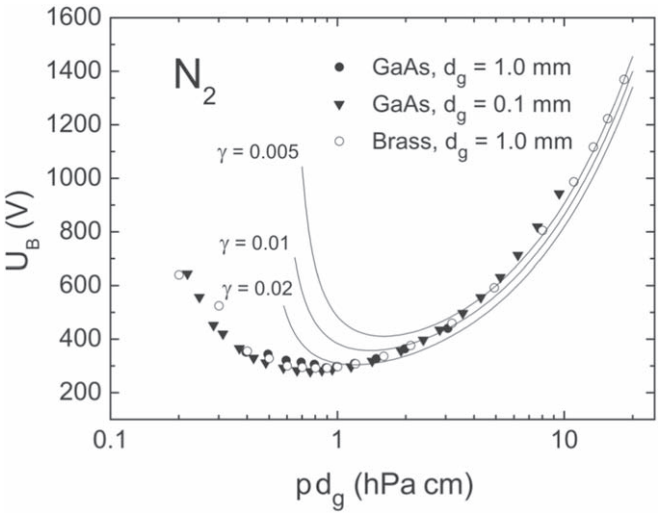

Figure 9. Paschen's curve for two cathode materials (GaAs and brass) in a plane-parallel structure. Reprinted with the permission of APS Publishing from [123]. Copyright 2014 American Physical Society.

that from a plane-parallel case having the shortest distance. If the protrusions are separated relatively far from each other, Paschen's curve will be flattened, similar to the tendency of the single protrusion case [117]. Paschen's curves were also measured in geometrically similar gaps with geometrically similar protrusions and it was found that the breakdown scaling law is still valid in the Townsend regime when the field emission doesn't come into play. The breakdown scaling laws are also verified for semiconductor materials. Reference [123] shows Paschen's curve measured for semiconductor (GaAs) and metal (brass) electrodes in nitrogen. In figure 9, the breakdown voltages for GaAs electrodes are obtained for interelectrode distance d_g of 1000 μm and 100 μm. The corresponding Paschen's curves are overlapping, which indicates the breakdown scaling laws are also valid for semiconductor materials. In figure 9, the breakdown voltage does not noticeably depend on the material, which was attributed to that the effective secondary electron emission was determined by an unspecified contamination layer of the cathode and other emission mechanisms by photons or excited atoms diffusing to the cathode [54, 124]. The key electrode emission process for this Townsend breakdown is the secondary electron emission from the cathode. More recently, experimental work by Brayfield *et al* on the impact of cathode surface roughness on microscale gas breakdown also considered the aging effect during

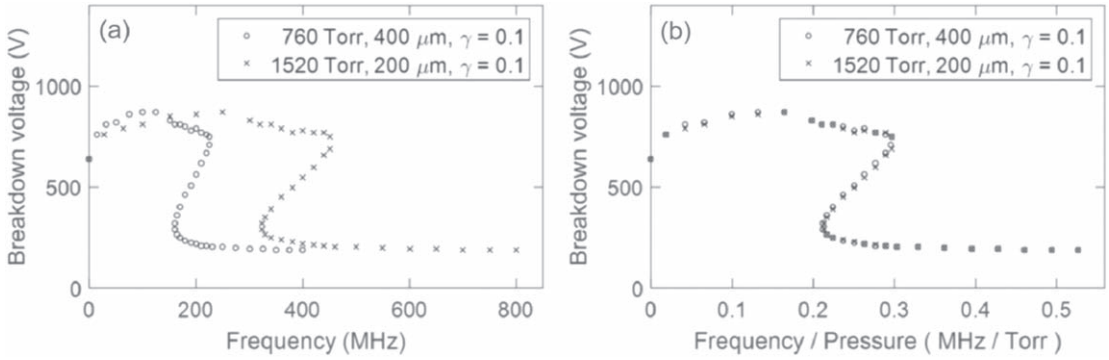

Figure 10. Breakdown curves obtained using PIC/MCC simulations. (a) Breakdown voltage versus frequency; (b) Breakdown voltage versus the ratio of frequency to gas pressure. Reprinted with the permission of IOP Publishing from [126]. Copyright 2017 Institute of Physics.

multiple breakdown events [125]. They observed a change in the dominant breakdown mechanism from field emission to Townsend avalanche to streamer in a single interelectrode gap ($d \leqslant 10$ μm) due to the formation of craters, which confirmed breakdown can be largely affected by the electrode surface status, especially during multiple-cycle operations.

Lee *et al* conducted Particle-in-cell/Monte Carlo collision (PIC/MCC) simulations of the breakdown curve with respect to an extended frequency scaling [126, 127]. Different from the former work in Ref. [112], in which Lisovskiy *et al* chose two different frequencies with varying pressures, Lee *et al* [126] swept a wide range of frequencies with two fixed pressures to obtain the extended breakdown scaling laws. However, the similarity law parameters for this extended Paschen's law are still the same as f/p and pd mentioned before. Or more specifically, relations $f_1/p_1 = f_2/p_2$ and $p_1d_1 = p_2d_2$ should be maintained for two compared gaps. It can be observed that in figure 10(a) the breakdown curves versus frequency are separated while in figure 10(b) the breakdown curves versus frequency divided by gas pressure are overlapping. The 'Z' or 'S' shaped Paschen's curve for RF driven sources should be measured using different parametric methods, which was discussed in Refs. [112, 128]. In high-pressure RF discharge in microgaps, the general breakdown characteristics are similar to the low-pressure RF discharge in larger gaps unless the field or thermionic emission appears; the scaling parameters for high-frequency gas breakdown are still pd, f/p, and d/R [126, 127].

4.2. Micro/nano scale breakdown

In the previous studies, it was confirmed that field emission will generally come into play for breakdown when the gap distance is less than 10 μm. Field emission is caused by either surface roughness with local field enhancement, by sufficiently decreased electrode distance, or by plasma sheath electric field enhancement with space charge effects [129–136]. In Refs. [130–133], Ramilović-Radjenović and Radjenović derived a mathematical model for microgap breakdown by introducing an ion-enhanced field emission coefficient, similar to the Townsend criteria, which was validated by PIC/MCC simulations. However, this model will overestimate the breakdown voltage when the breakdown transitions from field emission to ion-impact secondary electron emission with increasing gap distance. Later in Refs. [134, 135], Go *et al* derived an improved mathematical model with the two emission coefficients (field emission coefficient γ_{FE} and secondary electron emission coefficient γ_{se}) combined, which qualitatively represents the modified Paschen's curve, transiting from a field emission to a secondary electron emission regime, as shown in figure 11. The contribution from ion-enhanced field emission and ion-impact secondary electron emission can be represented by the coefficients and their ratios. Figure 11(b) shows the contribution from field emission is negligible when the gap distance is larger than 8 μm, which is consistent with the deviation from the classical Paschen's curve in figure 11(a). Although the model shows a fairly good agreement between the PIC simulations and experimental data, there are still some limitations, e.g. the space charge effect is not included. In Ref. [136], the contributions from three key mechanisms including electron impact ionization, secondary electron emission, and field emission are compared by using PIC/MCC simulations. Venkattraman derived a 1D model by using a Taylor expansion approximation and the space charge effect is incorporated by assuming constant charge density distributed from the gap center to the electrode [93]. The breakdown scaling was discussed with the consideration of electron backward scattering with modified ionization coefficient in the field emission regimes. Combining ion enhanced field emission and Fowler-Nordheim current density, Loveless *et al* made extensive efforts exploring a universal scaling law for gas breakdown from microscale to nanoscale [137–139]. By defining dimensionless variables for the breakdown condition, they obtained the dimensionless breakdown voltage versus the

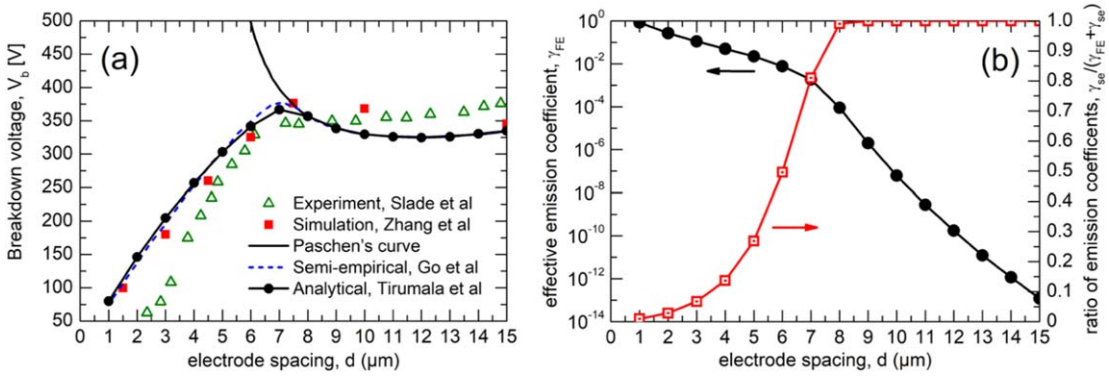

Figure 11. (a) Breakdown voltage versus the electrode spacing from 15 μm to 1 μm. The experimental data by Slade *et al* is from Ref. [77], the simulation data by Zhang *et al* is from Ref. [129], the semi-empirical model by Go *et al* is equation (1) from Ref. [134], and the analytical model by Tirumala *et al* is equation (7) from Ref. [135]. (b) The effective secondary emission coefficient and the normalized contribution of secondary emission versus the electrode spacing from 15 μm to 1 μm. Reproduced with the permission of AIP Publishing from [135].

normalized gas pressure, which is found to be overlapping for various gases (an average percent difference is ~1.6%), such as argon, nitrogen, neon, and xenon [137]. The breakdown condition derived with normalized variables is considered as a universal equation for dimensionless breakdown voltage without any material dependence. More recently, Loveless *et al* have also derived closed form solutions that show scaling with gap distance when field emission drives gas breakdown at microscale [140].

Experimentally, Peschot *et al* investigated the deviations from Paschen's curve at short gap distance d from 100 nm to 10 μm, by using a high precision electrode positioning system [141]. They found the deviation occurs when $d < 4$ μm and the plateau of Paschen's curve close to the field emission regime is confirmed with different breakdown criterions, i.e., $i_b > 50$ nA and $i_b > 1$ μA, as shown in figure 12. Even though the overall shape of Paschen's curve is not affected by the criteria used, the breakdown voltage is slightly modified. In their experiments, they observed two different breakdown behaviors, called 'direct' and 'progressive' breakdown, corresponding to the way the discharge current increases either abruptly or progressively. They attributed the plateau of Paschen's curve to the fact that the breakdown does not occur along the shortest gap distance with $1\ \mu\text{m} < d < 4\ \mu\text{m}$, as shown in figure 12(b). The breakdown could first occur along the shortest path I and then transitions to a longer path II, which maintains a roughly constant breakdown voltage, similar to the flattened Paschen's curve shown in figure 8(b). When d is less than 1 μm, the field emission becomes important due to the sufficiently high electric field ~10^9 V m^{-1}, due to the electric field enhancement caused by surface roughness or protrusions, as illustrated in figure 12(c). It should be noted that the breakdown path evolution in the non-field emission region, such as Townsend breakdown, could be caused by either the gas pressure or surface perturbations, which has been confirmed both numerically and experimentally [119, 122, 142]. However, the breakdown path evolution for explaining the plateau of Paschen's curve close to the field emission regime are not fully understood yet. It was proposed that the combination of a streamer and a glow discharge could also be a factor causing the constant breakdown voltage [143].

More recently, Meng *et al* [144, 145] carried out an *in-situ* electrical-optical diagnostic of dynamic breakdown process in interelectrode microgaps, as shown in figure 13. They found the breakdown propagated along the shortest distance between the electrodes with $d = 20$ μm, 15 μm, and 12 μm, corresponding to figures 13(a)–(c), respectively. However, the breakdown follows a curved line rather than the shortest straight line, as shown in figures 13(d)–(f), which was considered as the mechanism for the deviation from the theoretical prediction of the right branch of the Paschen's curve. In smaller gaps with $d = 3$ μm, 2 μm, and 1 μm, no obvious channels were observed since the discharge is diffuse, as shown in figures 13(g)–(i). They also showed that the emitted electrons can drift from the cathode to the anode directly since the mean free path and gap distance are comparable. The Nottingham heating effect could be a significant role for causing very high local temperatures and metal evaporation, which is also like the illustration in figure 12(c).

Even though the deviation from Paschen's law was extensively confirmed with metal interelectrode distance generally less than 10 μm, there are also some cases with non-metal electrodes where Paschen's law still holds for very small electrode gaps, as shown in figure 14. This work was carried out with silicon electrodes by Ono *et al* in Ref [146] and Chen *et al* in Ref [147] and was summarized by Go *et al* in a comprehensive review [148]. No deviation from Paschen's curve was observed for gap distances decreasing to 2 μm, which was attributed to the fact that silicon is a very poor field emitter compared to metals. This may explain why higher voltages are required to achieve breakdown on the left branch in figure 14, since there is insufficient electron emission from

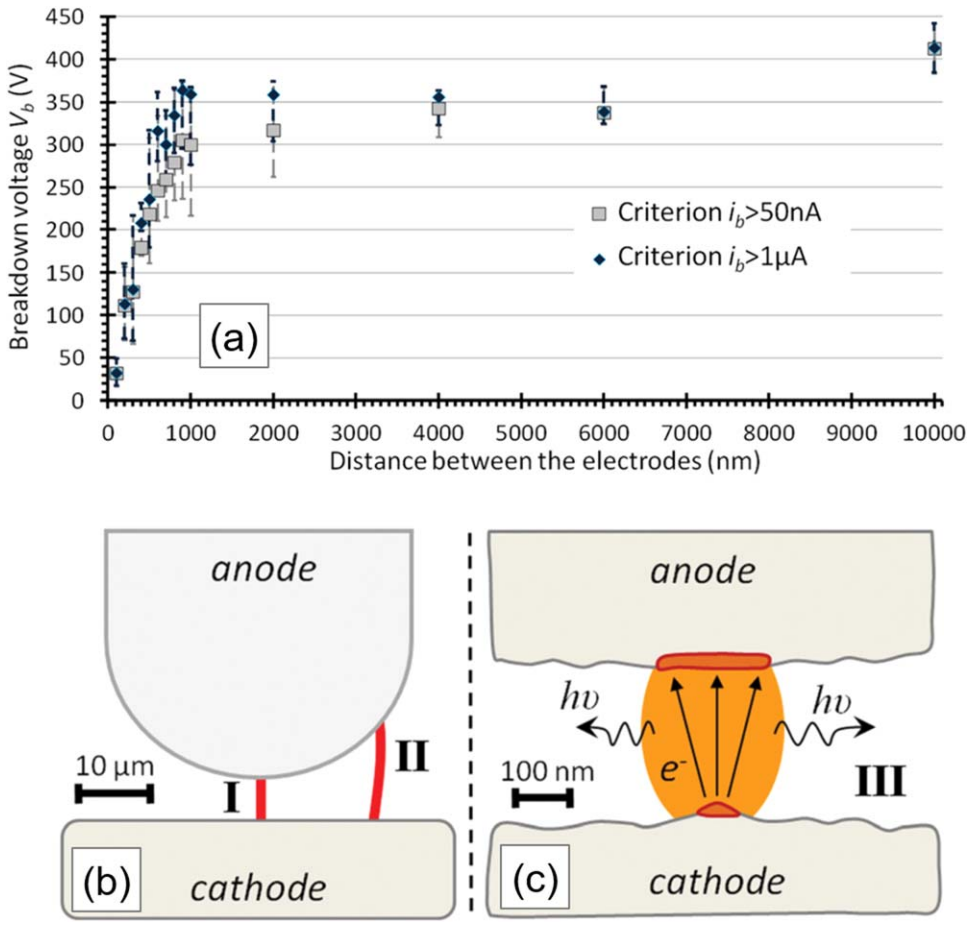

Figure 12. (a) Breakdown voltage measured with Ru Plate in air with different breakdown criteria and breakdown plateau is observed for $1\ \mu m < d < 4\ \mu m$; (b) Illustration of a breakdown path evolution explaining the breakdown plateau with $d > 1\ \mu m$; (c) Breakdown dominated by field emission with $d < 1\ \mu m$ to nanoscales. Reproduced with the permission of AIP Publishing from [141].

the cathode process. They also found that p-type silicon requires higher breakdown voltages than n-type silicon with the same electrode geometries. They attributed this to the fact that n-doping adds electrons to the conduction band while p-doping does not, leading to p-type having a smaller effective secondary electron emission coefficient [147, 148].

To extend the breakdown dynamics from DC to time-varying fields in microgaps, Semnani *et al* studied the frequency response of atmospheric pressure microgap gas breakdown by using PIC/MCC simulations [149]. Three scenarios with four typical regimes are observed with dependences on the gap distance, gas composition, and the amplitude and the frequency of the alternative applied field, as shown in figure 15. When the frequency is sufficiently low, most of the electrons and ions can reach and become lost to the electrode in each half cycle; this is referred to as the low frequency breakdown regime, with a variation of the breakdown voltage versus frequency less than 10% up to 5 GHz, as shown in figure 15(a). In this boundary-controlled regime, the breakdown is governed by the electrode processes, such as field emission and secondary electron emission. As the frequency increases close to the critical frequency, the breakdown voltage decreases sharply, showing a transition from the boundary to the diffusion-controlled regime. When the frequency is increased above critical frequency, i.e., $\sim$ 6 GHz, the breakdown voltage is almost constant, and it is referred as diffusion-controlled regime, since the primary electron loss mechanism is diffusion. Finally, if the frequency is further increased, the electrons cannot respond instantly to the fast oscillating field to gain enough energy to ionize the gas, thus a high amplitude of the applied voltage is required to trigger an avalanche breakdown, which is referred as the inertia controlled regime. The characteristics of the frequency response can be largely affected by the gap distance, as shown in figure 15(b). For the cases with gap distance of 0.5 μm and 2 μm, no obvious transition versus frequency is observed and the breakdown voltage is kept almost constant. This is because the breakdown is dominated by field emission and the variation of the breakdown voltage with frequency is negligible. The larger the gap, the more pronounced is the change of the breakdown voltage. For a gap distance of hundreds of microns, the breakdown voltage scaling with frequency would be similar to the results in figure 10. In the field emission regime, the breakdown voltage tends to be independent of the frequency; the electron-neutral

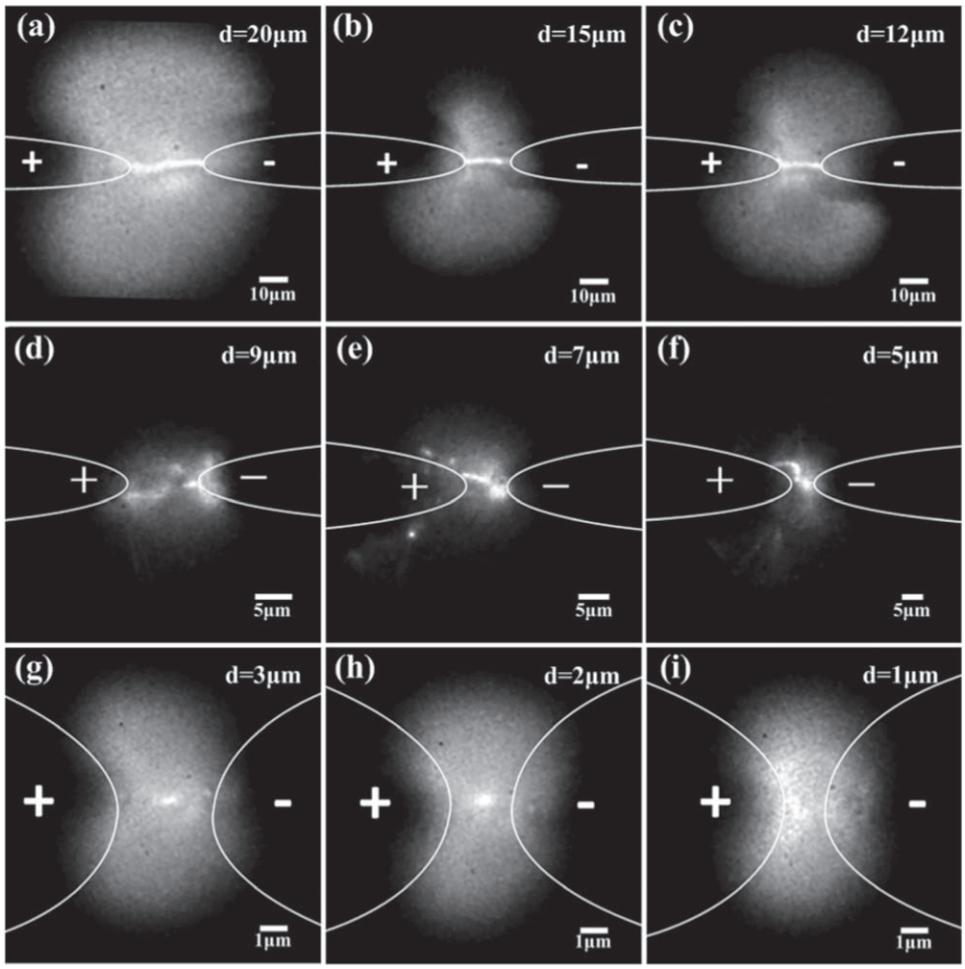

Figure 13. Breakdown morphology in a sphere-sphere gap with gap distance varying from 20 μm to 1 μm. (a)–(c) Breakdown propagating along the shortest path from tip to tip; (d)–(f) breakdown occurs with curve path and roughly constant length corresponds to the breakdown plateau; (g)–(i) no obvious breakdown channels are observed and the discharges are more diffuse-like. Reprinted with the permission of AIP Publishing from [144]. Copyright 2018 AIP Publishing LLC.

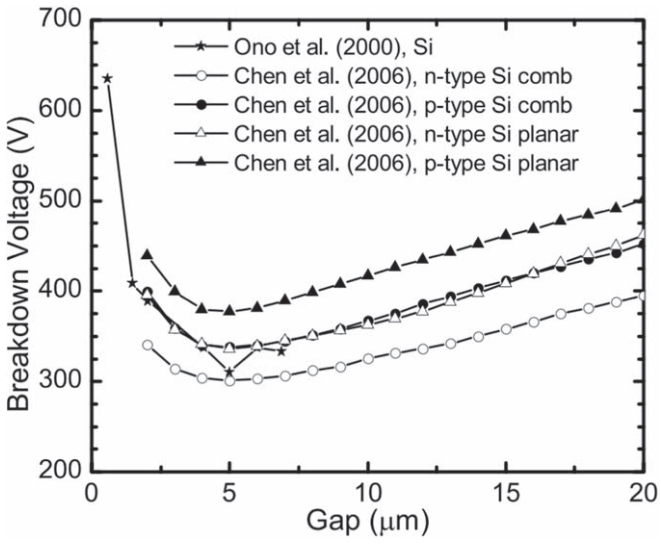

Figure 14. Breakdown voltage in ambient air at atmospheric pressure as a function of gap distance for various silicon electrodes. original data was extracted from [146, 147]. Reprinted with the permission of IOP Publishing from Ref [148]. Copyright 2014 Institute of Physics.

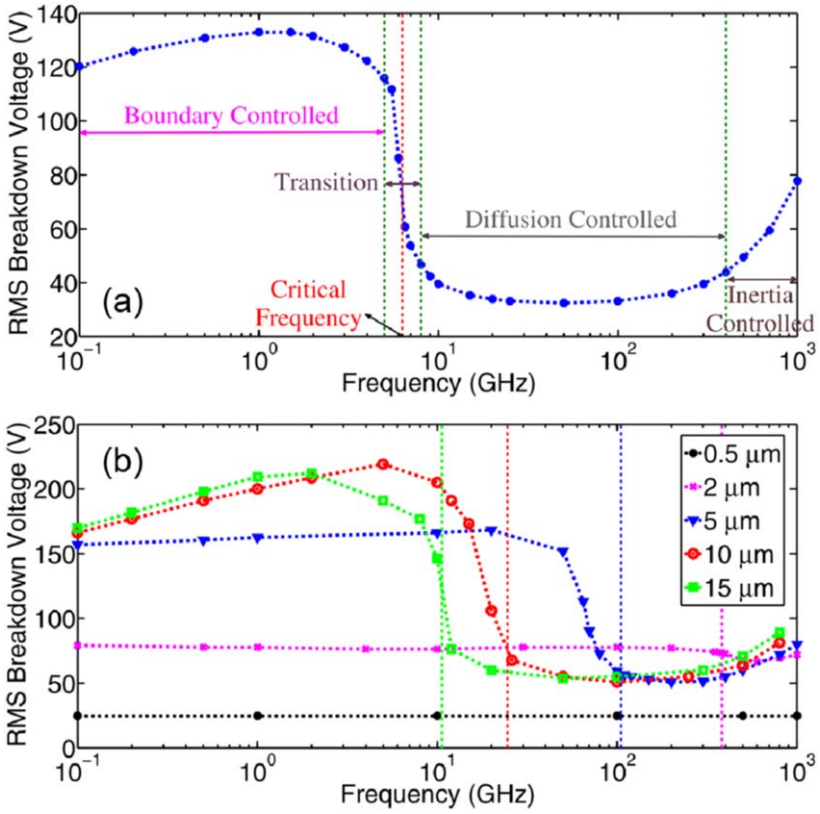

Figure 15. (a) The breakdown voltage dependence on frequency and the predicted critical frequency point in a 19 μm nitrogen gap with copper electrodes; (b) The breakdown voltage dependence on frequency and the predicted critical frequency point in 0.5 μm, 2 μm, 5 μm, 10 μm, and 15 μm argon gap with nickel electrodes. Reproduced with the permission of AIP Publishing from [149]. Copyright 2013 AIP Publishing LLC.

interaction is rare, and the electrons become ballistic, even up to atmospheric pressure. The electron emission current has a strong nonlinear dependence on the electric field. Thus, the classical breakdown scaling for AC discharges can hardly be obtained in the field emission regime.

As mentioned before, cold field emission could be the dominant electron source when the electric field is sufficiently high. However, thermionic emission can also become important if the cathode is heated to a high temperature. The classical thermal emission can be described by the Richardson-Dushman equation, without Schottky effect by the electric field [8, 150, 151]. The Schottky model should be used when an external voltage is applied across the gap. Improved emission models, such as field enhanced thermionic emission which incorporates the thermionic emission with Schottky effect and thermo-field emission which includes both thermionic and field emissions, were developed [8, 49]. Haase and Go incorporated two emission models, i.e., the Schottky emission model and the thermo-field emission model, to evaluate the impact of thermal emission on the breakdown and discharge properties at microscale dimensions [152]. Note that the Schottky emission model assumes modest electric field, thus it is also called the 'low-field' Schottky emission model. If the electric field is sufficiently high ($> \sim 5 \times 10^9$ V m^{-1}), the Schottky equation will underestimate the emission current. In this scenario, the complete Murphy-Good expression with multiple elliptic integrals should be employed, which is generally valid over the thermo-field regime [150–152]. For a faster computation , Haase and Go employed an approximate form developed by Hantzsche instead of the complete Murphy-Good expression [152, 153]. By comparing the emission models, they found the critical electric field value of $\sim 5 \times 10^9$ V m^{-1}, below which the Schottky expression is more accurate and above which Hantzsche's approximation is more accurate. The effect of the temperature on the breakdown curve, i.e., breakdown voltage as a function of *Nd* (gas number density $\times$ gap distance), is shown in figure 16. At lower cathode temperature (1000 °C), the breakdown curve first follows Paschen's curve at larger gaps and then falls below Paschen's curve at smaller gaps since the electric field becomes higher and causes larger emission. In the large gap regime, the thermionic emission at 1000 °C does not have a significant impact since the breakdown curve is overlapping with the prediction of Paschen's law. In the short-gap regime, the breakdown voltage decreases as expected from the modified Paschen's curve with field emission incorporated. At higher cathode temperature (1750 °C), the breakdown curve is completely below Paschen's curve, showing an increased deviation. In the large gap regime, besides the secondary electron emission, the thermionic emission becomes considerable and lowers the breakdown voltage.

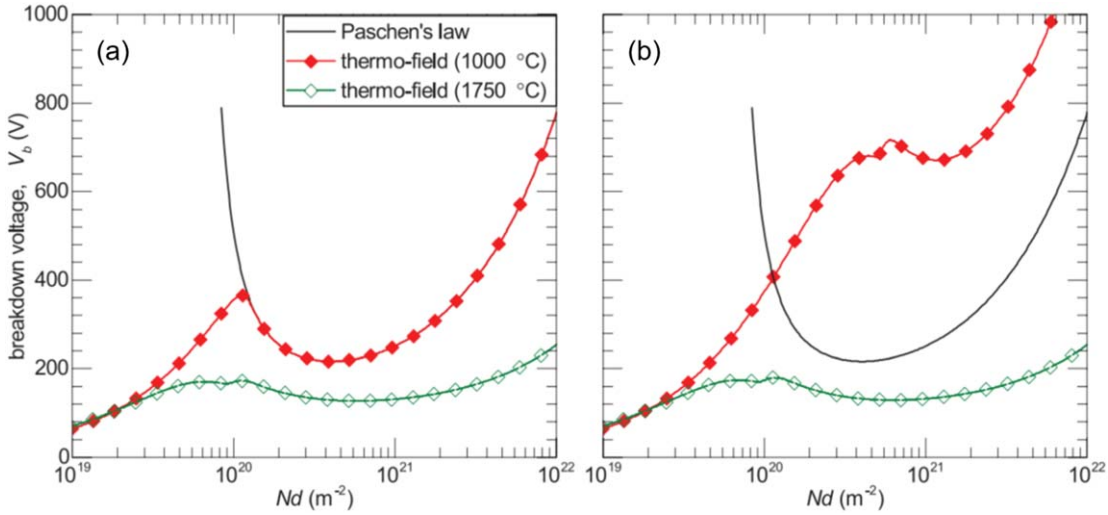

Figure 16. Breakdown voltage as a function of *Nd* (gas number density × gap distance) at a constant density of 6.3×10^{24} m^{-3} with cathode temperature at 1000 °C and 1750 °C. The electrode gap *d* varied from 1 μm to 2 mm. (a) $\gamma_{se} = 0.01$ (b) $\gamma_{se} = 0$. For comparison, Paschen's curve with $\gamma_{se} = 0.01$ is included on both (a) and (b). Reprinted with the permission of IOP Publishing from [152]. Copyright 2016 Institute of Physics.

In the short gap regime, the thermal emission is more sensitive to the space charge effect at higher temperatures, thus the total emission becomes more effective. The two effects work together to shift the breakdown curve further below, as shown in figure 16(a). In figure 16(b), the effect of the thermal emission could be evaluated more clearly by setting the secondary electron emission to zero, i.e., $\gamma_{se} = 0$. The breakdown curve corresponding to 1750 °C is almost the same, which indicates the thermal emission alone produces the breakdown behaviors and the contribution from the secondary electron emission is not important in this regime. Also, note that in figures 16 (a) and (b) for the 1000 °C case, the breakdown curve is roughly the same with and without secondary electron emission before the intersection with the classical Paschen's curve. After that intersection, a much higher breakdown voltage is required since the secondary electron emission is removed, and thermionic emission is not significant at 1000 °C.

Venkattraman proposed a generalized criterion based on the Townsend theory by considering thermionic and field emission simultaneously and used it to predict breakdown characteristics versus gap distance and cathode temperature in a 2D plot [154]. As shown in figure 17, the breakdown voltage was found to be a non-monotonic function of both cathode temperature and gap size. From the horizontal axis, the contour line is parallel to the temperature axis for very small gaps, which indicates the field emission is the dominant mechanism and the breakdown voltage is not affected significantly even though the cathode temperature varies in a wide range. From the perspective of the vertical axis, the contour line is parallel to the gap axis at high temperatures, which indicates the thermionic emission is dominant and the breakdown voltage is almost independent of gap size. A contour peak region appears in regimes where the contributions from the field emission and thermionic emission are comparable. The proposed model in Ref [154] is a theoretical extension of classical breakdown. It will recover the Townsend breakdown criterion if the thermionic and field emission mechanisms are absent. It provides a constructive and useful framework with a first step analysis for electric field driven or thermo-field driven microdischarges.

5. Concluding remarks

The fundamental theory and research progress made in the past on the electrical breakdown are comprehensively reviewed from macro to micro/nano scales. The main mechanisms for the breakdown processes are avalanche ionization and cathode emission, including secondary electron emission, thermionic emission, and field emission, which work together to impact the breakdown characteristics. The electrode surface morphology and gap geometry, which result in local field enhancements, electric shielding effect, as well as the non-uniformity of electric field distribution across the gap, are found to be of critical importance on the breakdown characteristics in both macro and microscale regimes, such as leading to the flattened Paschen's curve. Extensive efforts were made for the breakdown mode transition from the Townsend to thermionic or field emission regime, which will inspire further development of microplasma devices driven by field or thermionic emissions. These devices show promising applications in microchips, sensors, and analytical chemistry, which are designed and enhanced to be

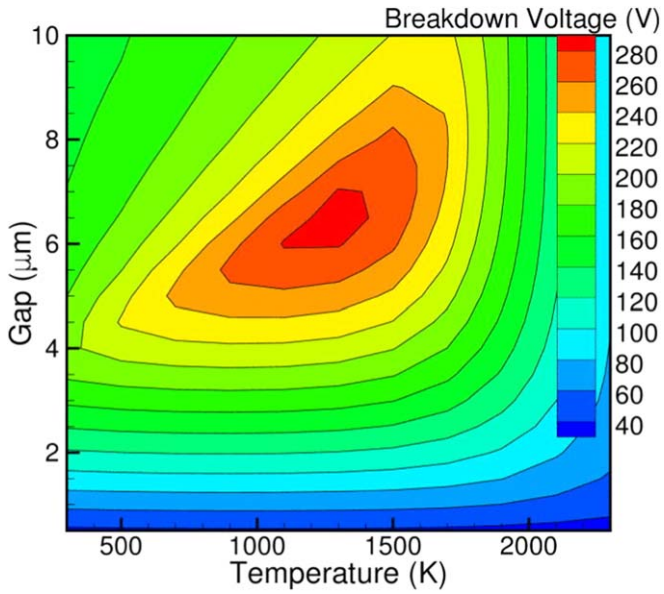

Figure 17. The breakdown voltage versus cathode temperature and gas distance, calculated based on the proposed model in Ref [154], for atmospheric pressure argon microdischarge. Reprinted with the permission of AIP Publishing from [154]. Copyright 2014 AIP Publishing LLC.

robust, reliable, and highly energy efficient. Their operation and tuning strategies could benefit from further breakdown investigations, which intrinsically provide the parameter sensitivities, system variabilities, and operating stabilities. With the development of microelectronics, scaling devices to smaller dimensions is a general trend, which is expected to further establish scaling laws both for the discharge breakdown and steady-state operation across a wide range of scales. The scaling characteristics will aid in applying the designation and optimization methods for the emerging plasma devices at various temporal and spatial scales. As for the plasma devices driven by DC, AC, and pulsed sources, controlling the operating modes and transition dynamics effectively is still challenging, and experimental optimizations, combined with numerical and theoretical efforts, provide new opportunities for more discoveries and practical applications.

Acknowledgments

This work was supported by the Air Force Office of Scientific Research (AFOSR) Grants FA9550-18-1-0062 and FA9550-18-1-0061, and the U.S. Department of Energy (DOE) Plasma Science Center Grant DE-SC0001939. Prof. Wang X also acknowledges the support of the National Natural Science Foundation Contract No. 51777114.

ORCID iDs

Yangyang Fu https://orcid.org/0000-0001-9593-3177
Peng Zhang https://orcid.org/0000-0003-0606-6855
John P Verboncoeur https://orcid.org/0000-0002-7078-3544
Xinxin Wang https://orcid.org/0000-0003-3564-6816

References

[1] Rao C R and Raju G R G 1971 Growth of ionization currents in dry air at high values of E/N *J. Phys. D: Appl. Phys.* **4** 494–503
[2] Kunhardt E E 1980 Electrical breakdown of gases: the prebreakdown stage *IEEE Trans. Plasma Sci.* **8** 130–8
[3] Nitta T and Nakanishi K 1991 Charge accumulation on insulating spacers for HVDC GIS *IEEE Trans. Dielectr. Electr. Insul.* **26** 418–27
[4] Larsson A 2012 Gas-discharge closing switches and their time jitter *IEEE Trans. Plasma Sci.* **40** 2431–42
[5] Wang H, Wandell R J, Tachibana K, Voráč J and Locke B R 2018 The influence of liquid conductivity on electrical breakdown and hydrogen peroxide production in a nanosecond pulsed plasma discharge generated in a water-film plasma reactor *J. Phys. D: Appl. Phys.* **52** 075201
[6] Osmokrović P, Živić T, Lončar B and Vasić A 2007 The validity of the similarity law for the electrical breakdown of SF_6 gas *IEEE Trans. Plasma Sci.* **35** 100–9
[7] Lisovskiy V A, Derevianko V A and Yegorenkov V D 2015 DC breakdown in low-pressure CF_4 *J. Phys. D: Appl. Phys.* **48** 475201

[8] Raizer Y P 1991 *Gas Discharge Physics* (New York: Springer)
[9] Paschen F 1889 Ueber die zum Funkenübergang in Luft, Wasserstoff und Kohlensäure bei verschiedenen Drucken erforderliche Potentialdifferenz *Ann. Phys.* **273** 69–96
[10] Townsend J S 1900 The conductivity produced in gases by the motion of negatively-charged ions *Nature* **62** 340–1
[11] Townsend J S 1915 *Electricity in Gases* (Oxford: Clarendon)
[12] Füllekrug M, Mareev E A and Rycroft M J 2006 *Sprites, Elves and Intense Lightning Discharges* (Dordrecht: Springer)
[13] Becker K H, Kogelschatz U, Schoenbach K H and Barker R J 2005 *Non-Equilibrium Air Plasmas at Atmospheric Pressure* (Bristol: IOP Publishing)
[14] Chen L, Widger P, Kamarudin M S, Griffiths H and Haddad A 2016 CF_3I gas mixtures: breakdown characteristics and potential for electrical insulation *IEEE Trans. Power Delivery* **32** 1089–97
[15] Park C, Graber L, Cheetham P, Al-Taie A, Telikapalli S and Pamidi S 2019 Versatile Paschen's model for the dielectric strength estimation of binary and ternary gas mixtures *IEEE Trans. Dielectr. Electr. Insul.* **26** 1569–76
[16] Osmokrovic P, Stojkanovic M, Stankovic K, Vujisic M and Kovacevic D 2012 Synergistic effect of SF_6 and N_2 gas mixtures on the dynamics of electrical breakdown *IEEE Trans. Dielectr. Electr. Insul.* **19** 677–88
[17] Abdel-kader M E, Gaber W H, Ebrahim F A and Al-Halim M A A 2019 Characterization of the electrical breakdown for DC discharge in Ar-He gas mixture *Vacuum* **169** 108922
[18] Pedersen A 1975 The effect of surface roughness on breakdown in SF_6 *IEEE Trans. Power Appar. Syst.* **94** 1749–54
[19] Berger S 1976 Onset or breakdown voltage reduction by electrode surface roughness in air and SF_6 *IEEE Trans. Power Appar. Syst.* **95** 1073–9
[20] Qiu Y and Chalmers I D 1993 Effect of electrode surface roughness on breakdown in SF_6-N_2 and SF_6-CO_2 gas mixtures *J. Phys. D: Appl. Phys.* **26** 1928–32
[21] Mesyats G A 2006 Similarity laws for pulsed gas discharges *Phys.-Usp.* **49** 1045–65
[22] Smith H B, Charles C and Boswell R W 2003 Breakdown behavior in radio-frequency argon discharges *Phys. Plasmas* **10** 875–81
[23] Levko D and Raja L L 2015 Breakdown of atmospheric pressure microgaps at high excitation frequencies *J. Appl. Phys.* **117** 173303
[24] Fujita H, Kouno T, Noguchi Y and Ueguri S 1978 Breakdown voltages of gaseous N_2 and air from normal to cryogenic temperatures *Cryogenics* **18** 195–200
[25] Massarczyk R, Chu P, Dugger C, Elliott S R, Rielage K and Xu W 2017 Paschen's law studies in cold gases *J. Instrum.* **12** P06019
[26] Hering M, Speck J, Großmann S and Riechert U 2017 Influence of gas temperature on the breakdown voltage in gas-insulated systems *IEEE Trans Dielectr. Electr. Insul.* **24** 401–8
[27] Cliteur G J, Hayashi Y, Haginomori E and Suzuki K 1998 Calculation of the uniform breakdown field strength of SF_6 gas *IEEE Trans. Dielectr. Electr. Insul.* **5** 843–9
[28] Fu Y, Krek J, Zhang P and Verboncoeur J P 2018 Evaluating microgap breakdown mode transition with electric field non-uniformity *Plasma Sources Sci. Technol.* **27** 095014
[29] Panchenko A N, Tarasenko V F, Beloplotov D V, Panchenko N A and Lomaev M I 2018 Diffuse discharges in SF_6 and mixtures of SF_6 with H_2, formed by nanosecond voltage pulses in non-uniform electric field *High Volt.* **3** 316–22
[30] Fu Y, Yang S, Zou X, Luo H and Wang X 2017 Effect of distribution of electric field on low-pressure gas breakdown *Phys. Plasmas* **24** 023508
[31] Buendia A and Venkattraman A 2015 Field enhancement factor dependence on electric field and implications on microscale gas breakdown: theory and experimental interpretation *Europhys. Lett.* **112** 55002
[32] Craighead H G 2000 Nanoelectromechanical systems *Science* **290** 1532–5
[33] Abeysinghe D C, Dasgupta S, Boyd J T and Jackson H E 2001 A novel MEMS pressure sensor fabricated on an optical fiber *IEEE Photonics Technol. Lett.* **13** 993–5
[34] Iwabuchi H, Oyama T, Kumada A and Hidaka K 2019 Breakdown phenomena across micrometer scale surface gap under negative voltage application *IEEE Trans. Dielectr. Electr. Insul.* **26** 1377–84
[35] Wang Q, Ning W, Dai D and Zhang Y 2019 How does the moderate wavy surface affect the discharge behavior in an atmospheric helium dielectric barrier discharge model? *Plasma Process Polym.* **16** e1900182
[36] Fu Y, Zhang P, Verboncoeur J P, Christlieb A J and Wang X 2018 Effect of surface protrusion on plasma sheath properties in atmospheric microdischarges *Phys. Plasmas* **25** 013530
[37] Chang C Y, Sasaki M, Kumagai S and Wang G J 2016 Design of microplasma electrodes for plasma-on-chip devices *J. Phys. D: Appl. Phys.* **49** 155203
[38] Chung J, Heo D, Shin G, Choi D, Choi K, Kim D and Lee S 2019 Ion-enhanced field emission triboelectric nanogenerator *Adv. Energy Mater.* **9** 1901731
[39] Fridman A and Kennedy L A 2004 *Plasma Physics and Engineering* (New York: Taylor & Francis)
[40] Gudmundsson J T and Hecimovic A 2017 Foundations of DC plasma sources *Plasma Sources Sci. Technol.* **26** 123001
[41] Ledernez L, Olcaytug F and Urban G 2012 Inter-electrode distance and breakdown voltage in low pressure argon discharges *Contrib. Plasma Phys.* **52** 276–82
[42] Burm K T A L 2007 Calculation of the Townsend discharge coefficients and the Paschen curve coefficients *Contrib. Plasma Phys.* **47** 177–82
[43] Engel A V 1965 *Ionized Gases* 2nd ed (London: Oxford University Press)
[44] Francis G 1960 *Ionization Phenomena in Gases* (London: Butterworths)
[45] Lieberman M A and Lichtenberg A J 2005 *Principles of Plasma Discharges and Materials Processing* (New York: Wiley)
[46] Davydov Y I 2006 On the first Townsend coefficient at high electric field *IEEE Trans. Nucl. Sci.* **53** 2931–5
[47] Kolobov V I and Godyak V A 1995 Nonlocal electron kinetics in collisional gas discharge plasmas *IEEE Trans. Plasma Sci.* **23** 503–31
[48] Kolobov V I and Godyak V A 2019 Electron kinetics in low-temperature plasmas *Phys. Plasmas* **26** 060601
[49] Go D B 2018 *Ionization and Ion Transport: A Primer for the Study of Non-Equilibrium, Low-Temperature Gas Discharges and Plasmas* (San Rafael: Morgan & Claypool Publishers)
[50] Kim H C and Verboncoeur J P 2006 Transition of window breakdown from vacuum multipactor discharge to rf plasma *Phys. Plasmas* **13** 123506
[51] Höhn F W J, Beckmann R and Wilhelm R 1997 The transition of a multipactor to a low-pressure gas discharge *Phys. Plasmas* **4** 940–4
[52] Kishek R A, Lau Y Y, Ang L K, Valfells A and Gilgenbach R M 1998 Multipactor discharge on metals and dielectrics: historical review and recent theories *Phys. Plasmas* **5** 2120–6
[53] Brown S C 1966 *Basic Data of Plasma Physics* (Cambridge: MIT Press)
[54] Phelps A V and Petrović Z L J 1999 Cold-cathode discharges and breakdown in argon: surface and gas phase production of secondary electrons *Plasma Sources Sci. Technol.* **8** R21–44

[55] Phelps A V and Jelenković B M 1988 Excitation and breakdown of Ar at very high ratios of electric field to gas density *Phys. Rev. A* **38** 2975–90
[56] Radmilović-Radjenović M, Matejčik Š, Klas M and Radjenović B 2012 The role of the field emission effect in direct-current argon discharges for the gaps ranging from 1 to 100 μm *J. Phys. D: Appl. Phys.* **46** 015302
[57] Hagstrum H D 1954 Theory of Auger ejection of electrons from metals by ions *Phys. Rev.* **96** 336–65
[58] Donkó Z 2001 Apparent secondary-electron emission coefficient and the voltage-current characteristics of argon glow discharges *Phys. Rev. E* **64** 026401
[59] Zheng B, Wang K, Shrestha M, Schuelke T and Fan Q H 2019 Understanding the chemical reactions in cathodic plasma electrolysis *Plasma Sources Sci. Technol.* **28** 085016
[60] Saheed M S M, Mohamed N M and Burhanudin Z A 2014 Breakdown voltage reduction by field emission in multi-walled carbon nanotubes based ionization gas sensor *Appl. Phys. Lett.* **104** 123105
[61] Donkó Z, Hartmann P and Kutasi K 2006 On the reliability of low-pressure dc glow discharge modelling *Plasma Sources Sci. Technol.* **15** 178–86
[62] Moon K S, Lee J and Whang K W 1999 Electron ejection from MgO thin films by low energy noble gas ions: energy dependence and initial instability of the secondary electron emission coefficient *J. Appl. Phys.* **86** 4049–51
[63] Aboelfotoh M O and Lorenzen J A 1977 Influence of secondary-electron emission from MgO surfaces on voltage-breakdown curves in Penning mixtures for insulated-electrode discharges *J. Appl. Phys.* **48** 4754–9
[64] Lisovskiy V A, Yakovin S D and Yegorenkov V D 2000 Low-pressure gas breakdown in uniform dc electric field *J. Phys. D: Appl. Phys.* **33** 2722–30
[65] Li L, Zhao Z, Liu Y, Li C, Ren J and Li J 2019 Repetitive gas-discharge closing switches for pulsed power applications *IEEE Trans. Plasma Sci.* **47** 4237–49
[66] Schoenbach K H and Becker K 2016 20 years of microplasma research: a status report *Eur. Phys. J. D* **70** 29
[67] Fu Y and Verboncoeur J P 2019 On the similarities of low-temperature plasma discharges *IEEE Trans. Plasma Sci.* **47** 1994–2003
[68] Becker K H, Schoenbach K H and Eden J G 2006 Microplasmas and applications *J. Phys. D: Appl. Phys.* **39** R55–70
[69] Iza F, Kong M G and Lee J K 2007 Electron kinetics in radio-frequency atmospheric-pressure microplasmas *Phys. Rev. Lett.* **99** 075004
[70] Schottky W 1914 Über den Austritt von Elektronen aus Glühdrähten bei verzögernden Potentialen *Ann. Phys. (Leipzig)* **44** 1011–32
[71] Fowler R and Nordheim L 1928 Electron emission in intense electric fields *Proc. R. Soc. A* **119** 173–81
[72] Murphy E L and Good R H 1956 Thermionic emission, field emission, and the transition region *Phys. Rev.* **102** 1464–73
[73] Jensen K L 2019 A reformulated general thermal-field emission equation *J. Appl. Phys.* **126** 065302
[74] Jensen K L 2007 General formulation of thermal, field, and photoinduced electron emission *J. Appl. Phys.* **102** 024911
[75] Jensen K L 2018 A tutorial on electron sources *IEEE Trans. Plasma Sci.* **46** 1881–99
[76] Kisliuk P 1954 Arcing at electrical contacts on closure: V. The cathode mechanism of extremely short arcs *J. Appl. Phys.* **25** 897–900
[77] Slade P G and Taylor E D 2002 Electrical breakdown in atmospheric air between closely spaced (0.2 μm–40 μm) electrical contacts *IEEE Trans. Compon. Packag. Tech.* **25** 390–6
[78] Radmilović-Radjenović M, Lee J K, Iza F and Park G Y 2005 Particle-in-cell simulation of gas breakdown in microgaps *J. Phys. D: Appl. Phys.* **38** 950–4
[79] Zuber K 1925 Über die Verzögerungszeit bei der Funkenentladung *Ann. Phys. (Leipzig)* **76** 231–60
[80] Von Laue M 1925 Bemerkung zu K. Zubers messung der verzögerungszeiten bei der funkenentladung *Ann. Phys. (Leipzig)* **76** 261–5
[81] Pejovic M M, Ristic G S and Karamarkovic J P 2002 Electrical breakdown in low pressure gases *J. Phys. D: Appl. Phys.* **35** R91–103
[82] Pejović M M and Filipović R D 1989 Method for determining the breakdown voltage in gas-filled tubes *Int. J. Electron.* **67** 251–6
[83] Ionikh Y Z, Meshchanov A V and Ivanov D O 2019 Dependence of the breakdown potential on the voltage rise rate in a long discharge tube at low pressure *Tech. Phys.* **64** 950–6
[84] Shishpanov A I, Ivanov D O and Kalinin S A 2019 Collision of ionization waves in long discharge tubes *Plasma Res. Express* **1** 025004
[85] Gendre M F, Haverlag M and Kroesen G W M 2010 Optical and electrostatic potential investigations of electrical breakdown phenomena in a low-pressure gas discharge lamp *J. Phys. D: Appl. Phys.* **43** 234004
[86] Dmitry L, Arslanbekov R R and Kolobov V I 2019 Modified Paschen curves for pulsed breakdown *Phys. Plasmas* **26** 064502
[87] Marić D, Hartmann P, Malović G, Donkó Z and Petrović Z L J 2003 Measurements and modelling of axial emission profiles in abnormal glow discharges in argon: heavy-particle processes *J. Phys. D: Appl. Phys.* **36** 2639–48
[88] Bilici M A, Haase J R, Boyle C R, Go D B and Sankaran R M 2016 The smooth transition from field emission to a self-sustained plasma in microscale electrode gaps at atmospheric pressure *J. Appl. Phys.* **119** 223301
[89] Rafatov I and Yesil C 2018 Transition from homogeneous stationary to oscillating state in planar gas discharge–semiconductor system in nitrogen: Effect of fluid modelling approach *Phys. Plasmas* **25** 082107
[90] Gocić S, Škoro N, Marić D and Petrović Z L J 2014 Influence of the cathode surface conditions on V–A characteristics in low-pressure nitrogen discharge *Plasma Sources Sci. Technol.* **23** 035003
[91] Petrović Z L J, Škoro N, Marić D, Mahony C M O, Maguire P D, Radmilović-Rađenović M and Malović G 2008 Breakdown, scaling and volt–ampere characteristics of low current micro-discharges *J. Phys. D: Appl. Phys.* **41** 194002
[92] Go D B 2013 Theoretical analysis of ion-enhanced thermionic emission for low-temperature, non-equilibrium gas discharges *J. Phys. D: Appl. Phys.* **46** 035202
[93] Venkattraman A and Alexeenko A A 2012 Scaling law for direct current field emission-driven microscale gas breakdown *Phys. Plasmas* **19** 123515
[94] Kudrle V, LeDuc E and Fitaire M 1999 Breakdown delay times and memory effects in helium at low pressure *J. Phys. D: Appl. Phys.* **32** 2049–55
[95] Jones J P, Llewellyn J P and Lewis T J 2005 The contribution of field-induced morphological change to the electrical aging and breakdown of polyethylene *IEEE Trans. Dielectr. Electr. Insul.* **12** 951–66
[96] Spasić I V, Radović M K, Pejović M M and Maluckov Č A 2003 The statistical time-delay and the breakdown formative time contributions to the memory effect in Ne at 7 mbar pressure *J. Phys. D: Appl. Phys.* **36** 2515–20
[97] Shao T, Sun G, Yan P, Wang J, Yuan W, Sun Y and Zhang S 2006 An experimental investigation of repetitive nanosecond-pulse breakdown in air *J. Phys. D: Appl. Phys.* **39** 2192–7
[98] Fu Y, Yang S, Zou X, Luo H and Wang X 2016 Similarity of gas discharge in low-pressure argon gaps between two plane-parallel electrodes *High Volt.* **1** 86–9
[99] Fu Y, Wang X, Zou X, Yang S, Verboncoeur J P and Christlieb A J 2017 Investigation on the similarity law of low-pressure glow discharges based on the light intensity distributions in geometrically similar gaps *Phys. Plasmas* **24** 083510

[100] Mathew P, George J, Mathews T S and Kurian P J 2019 Experimental verification of modified Paschen's law in DC glow discharge argon plasma *AIP Adv.* **9** 025215
[101] Fu Y, Krek J, Wen D, Zhang P and Verboncoeur J P 2019 Transition of low-temperature plasma similarity laws from low to high ionization degree regimes *Plasma Sources Sci. Technol.* **28** 095012
[102] Fu Y, Luo H, Zou X and Wang X 2014 Validity of the similarity law for the glow discharges in non-plane-parallel gaps *Plasma Sources Sci. Technol.* **23** 065035
[103] Wang X and Fu Y 2014 Similarity in gas discharges *High Volt. Eng.* **40** 2966–72
[104] Lisovskiy V A and Yakovin S D 2000 Scaling law for a low-pressure gas breakdown in a homogeneous DC electric field *JETP Lett.* **72** 34–7
[105] Lisovskiy V A, Osmayev R O, Gapon A V, Dudin S V, Lesnik I S and Yegorenkov V D 2017 Electric field non-uniformity effect on dc low pressure gas breakdown between flat electrodes *Vacuum* **145** 19–29
[106] Margenau H 1948 Theory of high frequency gas discharges: IV. Note on the similarity principle *Phys. Rev.* **73** 326–8
[107] Rukhadze A A, Sobolev N N and Sokovikov V V 1991 Similarity relations for low-temperature nonisothermal discharges *Sov. Phys. Usp.* **34** 827–9
[108] Holm R 1924 Der gegenwärtige Stand der Theorie des Glimmstroms *Phys. Z.* **25** 497–535
[109] Lisovskiy V A, Booth J P, Landry K, Douai D, Cassagne V and Yegorenkov V 2008 Similarity law for rf breakdown *Europhys. Lett.* **82** 15001
[110] Woo R and Ishimaru A 1967 A similarity principle for multipacting discharges *J. Appl. Phys.* **38** 5240–4
[111] Lau Y Y, Verboncoeur J P and Kim H C 2006 Scaling laws for dielectric window breakdown in vacuum and collisional regimes *Appl. Phys. Lett.* **89** 261501
[112] Puač M, Marić D, Radmilović-Radjenović M, Šuvakov M and Petrović Z L J 2018 Monte Carlo modeling of radio-frequency breakdown in argon *Plasma Sources Sci. Technol.* **27** 075013
[113] Fu Y, Parsey G M, Verboncoeur J P and Christlieb A J 2017 Investigation on the effect of nonlinear processes on similarity law in high-pressure argon discharges *Phys. Plasmas* **24** 113518
[114] Nam S K and Verboncoeur J P 2009 Global model for high power microwave breakdown at high pressure in air *Comput. Phys. Commun.* **180** 628–35
[115] Nam S K, Lim C H and Verboncoeur J P 2009 Dielectric window breakdown in oxygen gas: Global model and particle-in-cell approach *Phys. Plasmas* **16** 023501
[116] Fu Y, Yang S, Zou X, Luo H and Wang X 2016 Intersection of Paschen's curves for argon *Phys. Plasmas* **23** 093509
[117] Fu Y, Zhang P and Verboncoeur J P 2018 Paschen's curve in microgaps with an electrode surface protrusion *Appl. Phys. Lett.* **113** 054102
[118] Fu Y, Zhang P and Verboncoeur J P 2018 Gas breakdown in atmospheric pressure microgaps with a surface protrusion on the cathode *Appl. Phys. Lett.* **112** 254102
[119] Fu Y, Krek J, Zhang P and Verboncoeur J P 2019 Gas breakdown in microgaps with a surface protrusion on the electrode *IEEE Trans. Plasma Sci.* **47** 2011
[120] Fu Y, Zhang P, Krek J and Verboncoeur J P 2019 Gas breakdown and its scaling law in microgaps with multiple concentric cathode protrusions *Appl. Phys. Lett.* **114** 014102
[121] Schnyder R, Howling A A, Bommottet D and Hollenstein C 2013 Direct current breakdown in gases for complex geometries from high vacuum to atmospheric pressure *J. Phys. D: Appl. Phys.* **46** 285205
[122] Yu B, Liang W, Jiao J, Kang X and Zhao Q 2019 Critical breakdown path under low-pressure and slightly uneven electric field gap *Acta Phys. Sin.* **68** 070201
[123] Astrov Y A, Lodygin A N and Portsel L M 2014 Dynamics and stability of the Townsend discharge in nitrogen in narrow gaps *Phys. Rev. E* **89** 033109
[124] Phelps A V 1960 Role of molecular ions, metastable molecules, and resonance radiation in the breakdown of rare gases *Phys. Rev.* **117** 619–32
[125] Brayfield R S, Fairbanks A J, Loveless A M, Gao S, Dhanabal A, Li W, Darr C, Wu W and Garner A L 2019 The impact of cathode surface roughness and multiple breakdown events on microscale gas breakdown at atmospheric pressure *J. Appl. Phys.* **125** 203302
[126] Lee M U, Lee J, Lee J K and Yun G S 2017 Extended scaling and Paschen law for micro-sized radiofrequency plasma breakdown *Plasma Sources Sci. Technol.* **26** 034003
[127] Lee M U, Lee J, Yun G S and Lee J K 2017 Scalings and universality for high-frequency excited high-pressure argon microplasma *Eur. Phys. J. D* **71** 94
[128] Lisovskiy V A, Martins S, Landry K, Douai D, Booth J P, Cassagne V and Yegorenkov V 2005 The effect of discharge chamber geometry on the ignition of low-pressure rf capacitive discharges *Phys. Plasmas* **12** 093505
[129] Zhang W, Fisher T S and Garimella S V 2004 Simulation of ion generation and breakdown in atmospheric air *J. Appl. Phys.* **96** 6066–72
[130] Radmilović-Radjenović M and Radjenović B 2007 The influence of ion-enhanced field emission on the high-frequency breakdown in microgaps *Plasma Sources Sci. Technol.* **16** 337–40
[131] Radmilović-Radjenović M and Radjenović B 2008 Theoretical study of the electron field emission phenomena in the generation of a micrometer scale discharge *Plasma Sources Sci. Technol.* **17** 024005
[132] Radmilović-Radjenović M and Radjenović B 2008 An analytical relation describing the dramatic reduction of the breakdown voltage for the microgap devices *Europhys. Lett.* **83** 25001
[133] Radmilović-Radjenović M, Matejčik Š, Klas M and Radjenović B 2013 The role of the field emission effect in direct-current argon discharges for the gaps ranging from 1 to 100 μm *J. Phys. D: Appl. Phys.* **46** 015302
[134] Go D B and Pohlman D A 2010 A mathematical model of the modified Paschen's curve for breakdown in microscale gaps *J. Appl. Phys.* **107** 103303
[135] Tirumala R and Go D B 2010 An analytical formulation for the modified Paschen's curve *Appl. Phys. Lett.* **97** 151502
[136] Semnani A, Venkattraman A, Alexeenko A A and Peroulis D 2013 Pre-breakdown evaluation of gas discharge mechanisms in microgaps *Appl. Phys. Lett.* **102** 174102
[137] Loveless A M and Garner A L 2017 A universal theory for gas breakdown from microscale to the classical Paschen law *Phys. Plasmas* **24** 113522
[138] Loveless A M and Garner A L 2016 Scaling laws for gas breakdown for nanoscale to microscale gaps at atmospheric pressure *Appl. Phys. Lett.* **108** 234103
[139] Loveless A M and Garner A L 2017 Generalization of microdischarge scaling laws for all gases at atmospheric pressure *IEEE Trans. Plasma Sci.* **45** 574–83
[140] Loveless A M, Meng G, Ying Q, Wu F, Wang K, Cheng Y and Garner A L 2019 The transition to Paschen's law for microscale gas breakdown at sub atmospheric pressure *Sci. Rep.* **9** 5669

[141] Peschot A, Bonifaci N, Lesaint O, Valadares C and Poulain C 2014 Deviations from the Paschen's law at short gap distances from 100 nm to 10 μm in air and nitrogen *Appl. Phys. Lett.* **105** 123109
[142] Marić D, Škoro N, Maguire P D, Mahony C M O, Malović G and Petrović Z L J 2012 On the possibility of long path breakdown affecting the Paschen curves for microdischarges *Plasma Sources Sci. Technol.* **21** 035016
[143] Osmokrovic P, Vujisic M, Stankovic K, Vasic A and Loncar B 2007 Mechanism of electrical breakdown of gases for pressures from 10^{-9} to 1 bar and inter-electrode gaps from 0.1 to 0.5 mm *Plasma Sources Sci. Technol.* **16** 643–55
[144] Meng G, Gao X, Loveless A M, Dong C, Zhang D, Wang K, Zhu B, Cheng Y and Garner A L 2018 Demonstration of field emission driven microscale gas breakdown for pulsed voltages using *in-situ* optical imaging *Phys. Plasmas* **25** 082116
[145] Meng G, Ying Q, Loveless A M, Wu F, Wang K, Fu Y, Garner A L and Cheng Y 2019 Spatio-temporal dynamics of pulsed gas breakdown in microgaps *Phys. Plasmas* **26** 014506
[146] Ono T, Sim D Y and Esashi J 2000 Micro-discharge and electric breakdown in a micro-gap *J. Micromech. Microeng.* **10** 445–51
[147] Chen C-H, Yeh J A and Wang P-J 2006 Electrical breakdown phenomena for devices with micron separations *J. Micromech. Microeng.* **16** 1366–73
[148] Go D B and Venkattraman A 2014 Microscale gas breakdown: ion-enhanced field emission and the modified Paschen's curve *J. Phys. D: Appl. Phys.* **47** 503001
[149] Semnani A, Venkattraman A, Alexeenko A A and Peroulis D 2013 Frequency response of atmospheric pressure gas breakdown in micro/nanogaps *Appl. Phys. Lett.* **103** 063102
[150] Herring C and Nichols M H 1949 Thermionic emission *Rev. Mod. Phys.* **21** 185–270
[151] Simmons J G 1965 Richardson-Schottky effect in solids *Phys. Rev. Lett.* **15** 967–8
[152] Haase J R and David B G 2016 Analysis of thermionic and thermo-field emission in microscale gas discharges *J. Phys. D: Appl. Phys.* **49** 055206
[153] Hantzsche E 1982 The thermo-field emission of electrons in arc discharges *Beiträge Aus Der Plasmaphys.* **22** 325–46
[154] Venkattraman A 2014 Generalized criterion for thermo-field emission driven electrical breakdown of gases *Appl. Phys. Lett.* **104** 194101
[155] Sahni O and Lanza C 1976 Importance of the dependence of the secondary electron emission coefficient on E/p_0 for Paschen breakdown curves in ac plasma panels *J. Appl. Phys.* **47** 1337–40
[156] Jensen Kevin L and Cahay M 2006 General thermal-field emission equation *Appl. Phys. Lett.* **88** 154105